AFIT/GA/AA/83D-1

DISCONTINUOUS LOW THRUST ORBIT TRANSFER

THESIS

John R. Cass, Jr.
Captain, USAF

AFIT/GA/AA/83D-1

Approved for public release; distribution unlimited

AFIT/GA/AA/83D-1

DISCONTINUOUS LOW THRUST ORBIT TRANSFER

THESIS

Presented to the Faculty of the School of Engineering
of the Air Force Institute of Technology
Air University
in Partial Fulfillment of the
Requirements for the Degree of
Master of Science

John R. Cass, Jr. B.S.
Captain, USAF

December 1983

Preface

The subject of low-thrust, ion rockets has interested me since I first learned of such vehicles in an undergraduate astrodynamics course. Air Force duties prevented me from keeping abreast of new developments over the past few years, however. I welcomed the opportunity of working on this subject for my thesis.

I would like to acknowledge the help of my advisor, Dr. William Wiesel. But I especially want to thank my wife and typist, Jan, for her understanding and help over the past 18 months. I also hope my two daughters, Laura and Leslie, will forgive me for the lack of attention they have had to experience.

Bob Cass

Table of Contents

	Page
Preface	ii
List of Figures	iv
List of Symbols	v
Abstract	vi
I. Introduction	1
II. Fast Timescale Problem	3
Derivation	3
Examples	18
III. Slow Timescale Problem	26
Problem Statement	26
Derivation	26
Implementation	38
IV. Results	42
Case I	42
Case II	46
Case III	47
Multiple Local Minima	48
General Observations	49
V. Conclusions and Recommendations	51
Bibliography	53
Vita	54

List of Figures

Figure		Page
1.	Shadow Boundaries	7
2.	Acceleration Components	10
3.	Sun-Orbit Geometrical Relationship	15
4.	Shadow Geometry	16
5.	Shadow Effects on λ_2	19
6.	Shadow Effects on Δa and Δi	20
7.	α and γ for m = 0	23
8.	α and γ for m = $\pi/6$	24
9.	α and γ for m = $\pi/3$	25
10.	λ_a and λ_i for Initial Conditions	40
11.	λ_a and λ_i for Final Conditions	40
12.	Case I	43
13.	Case II	44
14.	Case III	45
15.	Initial Conditions Case II	46
16.	Initial Conditions Case III	47
17.	τ versus $\lambda_{a(0)}$	49

List of Symbols

a	semi-major axis
a_f	final a
a_i	initial a
B	second position angle of anti-sun point
D	function of λ_1, λ_2, a, f, s
DU	earth distance unit
e	orbital eccentricity
f	true anomaly
F	integrand of performance index
F_σ	constant in computation of σ_o
g	true anomaly at shadow entry
G	universal gravitation constant
G_σ	constant in computation of σ_o
H	Hamiltonian
i	orbital inclination
i_f	final i
J	performance index
L	first position angle of anti-sun point
m	one-half actual shadow angle
$\dot{m}_p$	specific mass flow rate
$M_\oplus$	mass of earth
n	mean motion
$R_\odot$	angular semi-diameter of sun
s	angle between ascending node and shadow exit
t	time

T	total acceleration from thrust
T_0	initial T
TU	earth time unit
u	control variable
U	radial acceleration component
V	tangential acceleration component
W	normal acceleration component
X	$\partial m / \partial a$
Y	$\partial m / \partial i$
$\mathcal{P}$	orbital period of satellite
α	thrust angle in orbit plane
$\alpha_\odot$	right ascension of sun
γ	thrust angle out of orbit plane
$\delta_\odot$	declination of sun
λ	Lagrange multiplier
μ	gravitational parameter
π_s	parallex of satellite
$\pi_\odot$	parallex of sun
σ_0	one-half maximum shadow angle
τ	independent variable in slow timescale problem
ω	argument of perigee
Ω	longitude of the ascending node

Abstract

This paper examines the use of discontinuous low thrust for orbital transfers between two non-coplanar, circular orbits. The vehicle is assumed to be a solar-powered, ion rocket that cannot operate when it is within the earth's shadow. Two timescales are used to derive a minimum fuel trajectory. The fast timescale solution maximizes a change in inclination.when given a change in semi-major axis for a single orbit. The slow timescale solution combines fast timescale results to obtain the minimum fuel trajectory. Results are presented for three specific transfers requiring varying amounts of shadow penetration. It is shown that the fuel penalty caused by discontinuous thrust is very small. However, there can be a moderate increase in total trip time if the time within shadow is large.

DISCONTINUOUS LOW THRUST ORBIT TRANSFER

I Introduction

Electric propulsion research continues to seek new methods of accomplishing future missions in space.[1] Electrically propelled vehicles offer two important advantages for anticipated missions dealing with large space structures. One advantage is an increase in payload ratio which will allow more massive structures to be propelled. The other advantage comes from the extremely low acceleration available from electric thrusters. The large space structures being proposed will be flimsy and unable to withstand large accelerations. Electric propulsion offers a way of moving these large structures around in space.

Although there are many versions of electric thrusters, they all have common characteristics. The most notable are high specific impulse, low mass flow rate and low thrust. These devices provide thrust by electrically accelerating charged ions and then exhausting them into space.

Several authors (Alfano[2], Moeckel[3], Ehrike[4], and Stuhlinger[5]) have shown that the optimal trajectory for orbital transfers using continuous low thrust is an outward spiral. Alfano has derived an optimal control law to perform transfers that include changes in both inclination

and semi-major axis. All these solutions have been based on the use of continuous low thrust.

But continuous thrust may not be available. The electric power used to drive these thrusters will probably be produced by solar cells or a nuclear power plant. Since nuclear power sources weigh more per kilowatt than solar cells and since nuclear power is becoming less attractive in general, it is reasonable to assume that many of these vehicles will be solar-powered.[6] A solar-powered rocket has one serious disadvantage, however. It will not work when it is in the earth's shadow. Therefore, such a craft could not provide continuous thrust.

If tangential thrust were applied only when the vehicle is in sunlight, a circular orbit would not remain circular very long. Since the previous control schemes all assumed circular orbits would remain circular, they are not valid for discontinuous low thrust. This paper addresses the problem of using discontinuous low thrust for non-coplanar transfers between circular orbits.

The derivation is divided into two problems of differing time scales. The fast timescale problem optimizes the changes in orbital elements over one orbit with vehicle mass held constant. The slow timescale problem uses the results of the fast timescale optimization, while updating the mass and acceleration on each orbit.

II Fast Timescale Problem

The fast timescale problem addresses the changes in orbital elements that occur during one revolution of the central body. The solution should produce a thrust profile which will maximize a change in either inclination or semi-major axis when a particular change in the other is specified. Thrust application is only possible when the solar-powered spacecraft is in sunlight.

Derivation

The following derivation assumes two-body motion with the earth as the central body. Electric engines produce low thrust and hence cause only small changes in the orbital elements during one orbit. Consequently, general perturbation theory is used in that all the orbit elements are considered constant during each orbit. Also, fuel consumption is low enough that mass is considered constant during one orbit.

The equations of motion are given by Lagrange's planetary equations in their acceleration component form:[7]

$$\frac{d\Omega}{dt} = \frac{W\,(1-e^2)^{\frac{1}{2}}\sin(f+\omega)}{n\,a\,(1+e\cos f)\sin i} \tag{1}$$

$$\frac{di}{dt} = \frac{W\,(1-e^2)^{\frac{1}{2}}\cos(f+\omega)}{n\,a\,(1+e\cos f)} \tag{2}$$

$$\frac{d\omega}{dt} = \frac{-U\,(1-e^2)^{\frac{1}{2}}\cos f}{n\,a\,e} + \frac{V\,(1-e^2)^{\frac{1}{2}}(2 + e\cos f)\sin f}{n\,a\,e\,(1 + e\cos f)}$$

$$- \frac{W\,(1-e^2)^{\frac{1}{2}}\sin(f+\omega)\cot i}{n\,a\,(1 + e\cos f)} \qquad (3)$$

$$\frac{de}{dt} = \frac{U\,(1-e^2)^{\frac{1}{2}}\sin f}{n\,a}$$

$$+ \frac{V\,(1-e^2)^{\frac{1}{2}}}{n\,a\,e}\left[1 + e\cos f - \frac{1 - e^2}{1 + e\cos f}\right] \qquad (4)$$

$$\frac{da}{dt} = \frac{2\,U\,e\sin f}{n\,(1-e^2)^{\frac{1}{2}}} + \frac{2\,V\,(1 + e\cos f)}{n\,(1-e^2)^{\frac{1}{2}}} \qquad (5)$$

where a is the semi-major axis; e is the eccentricity; i is inclination; ω is the argument of perigee; Ω is the longitude of the ascending node; f is the true anomaly; U, V and W are the radial, tangential and normal acceleration components, respectively; and n is the mean motion.

$$n = (\mu/a^3)^{\frac{1}{2}} \qquad (6)$$

where

$$\mu = G\,M_{\oplus} \qquad (7)$$

and G is the universal gravitation constant and $M_{\oplus}$ is the

mass of the earth.

For transfers between circular orbits with continuous low thrust, many authors have shown that the optimum thrust profile requires negligible radial thrust. It has also been shown that the use of purely tangential thrust causes only negligible changes in eccentricity for transfers to geosynchronous altitude when the thrust acceleration is less than 10^{-3} g's.[5] But when thrust is applied over only part of the orbit, eventual changes in eccentricity can be expected. It is also possible that the optimum thrust profile would require that eccentricity be allowed to vary from zero. But the planetary equations can be greatly simplified if the dependence on eccentricity can be eliminated.

To eliminate eccentricity from the planetary equations, an additional constraint is added to the problem. It will be required that the change in eccentricity for each orbit be equal to zero. Since the initial orbit is circular, this constraint forces e to remain zero for the entire profile. Radial thrust will be used to negate changes in e that would be caused by pure tangential thrust.

Although this profile may not be the absolute optimum because of the additional constraint, it will be shown that it is at least near optimum.

The requirement that $e = 0$ causes the planetary equations to become

$$\frac{d\Omega}{dt} = \frac{W \sin(f+\omega)}{n\, a \sin i} \tag{8}$$

$$\frac{di}{dt} = \frac{W \cos(f+\omega)}{n\, a} \tag{9}$$

$$\frac{d\omega}{dt} \text{ is undefined for a circular orbit} \tag{10}$$

$$\frac{de}{dt} = \frac{U \sin f}{n\, a} + \frac{2\, V \cos f}{n\, a} \tag{11}$$

$$\frac{da}{dt} = \frac{2\, V}{n} \tag{12}$$

An explanation is in order as to why Eqs (8) and (9) contain ω, when the argument of perigee is undefined for circular orbits. In most problems dealing with circular orbits, ω is set equal to zero and then dropped from the equations. Implicit in this operation is that f will be measured from the ascending node, since ω in Eqs (8) and (9) represents a phase shift from the ascending node. In the derivation that follows, f will be measured from the point at which the spacecraft exits the earth's shadow. In this paper, shadow entry and exit points are considered the boundaries of the umbra. To avoid confusion, s will be used as the phase shift from the ascending node to the

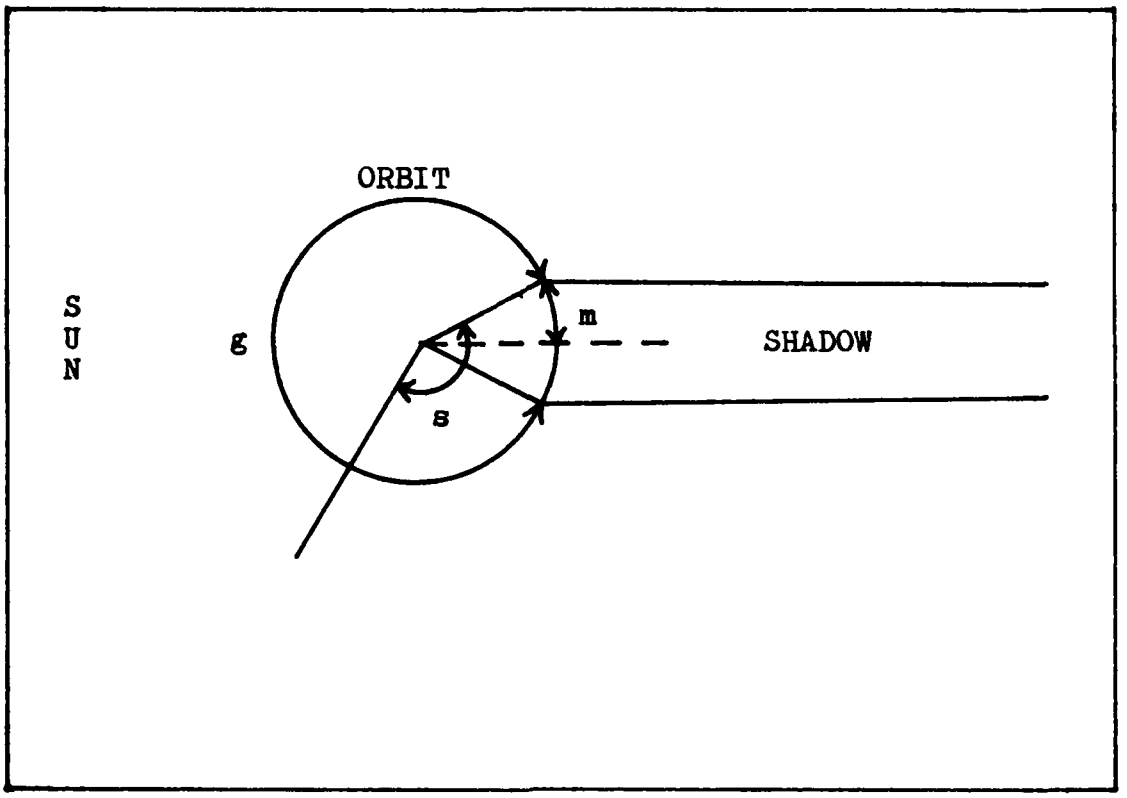

Fig. 1. Shadow Boundaries

shadow exit point. Also, g will be a measure of the angle from shadow exit to the next shadow entry and m will be one-half of the angle of shadow. See Figure 1 for a depiction of these angles. Substituting s for ω gives

$$\frac{d\Omega}{dt} = \frac{W \sin(f+s)}{n\, a \sin i} \tag{13}$$

$$\frac{di}{dt} = \frac{W \cos(f+s)}{n\, a} \tag{14}$$

Since $n = df/dt$, a change of independent variable can be

made from t to f. Substitution yields

$$\frac{d\Omega}{df} = \frac{W \sin(f+s)}{n^2 a \sin i} \tag{15}$$

$$\frac{di}{df} = \frac{W \cos(f+s)}{n^2 a} \tag{16}$$

$$\frac{de}{df} = \frac{U \sin f + 2 V \cos f}{n^2 a} \tag{17}$$

$$\frac{da}{df} = \frac{2 V}{n^2} \tag{18}$$

Substituting Eq (6) gives

$$\frac{d\Omega}{df} = \frac{W a^2 \sin(f+s)}{\mu \sin i} \tag{19}$$

$$\frac{di}{df} = \frac{W a^2 \cos(f+s)}{\mu} \tag{20}$$

$$\frac{de}{df} = \frac{a^2}{\mu}(U \sin f + 2 V \cos f) \tag{21}$$

$$\frac{da}{df} = \frac{a^3 2 V}{\mu} \tag{22}$$

To determine the changes in the orbital parameters for one orbit, these equations should be integrated from 0 to 2π . But U, V, and W are zero when the spacecraft is in shadow; so these equations can be integrated from 0 to g where g is the true anomaly at the point where the shadow is entered. The changes in orbital elements are then

$$\Delta\Omega = \int_0^g \frac{W\, a^2 \sin(f+s)\, df}{\mu \sin i} \tag{23}$$

$$\Delta i = \int_0^g \frac{W\, a^2 \cos(f+s)\, df}{\mu} \tag{24}$$

$$\Delta e = \int_0^g \frac{a^2}{\mu}(U \sin f + 2\, V \cos f)\, df \tag{25}$$

$$\Delta a = \int_0^g \frac{2\, V\, a^3\, df}{\mu} \tag{26}$$

The thrust accelerations U, V and W can be modeled as functions of f. From Figure 2,

$$U = T \cos\gamma \cos\alpha \tag{27}$$

$$V = T \cos\gamma \sin\alpha \tag{28}$$

$$W = T \sin\gamma \tag{29}$$

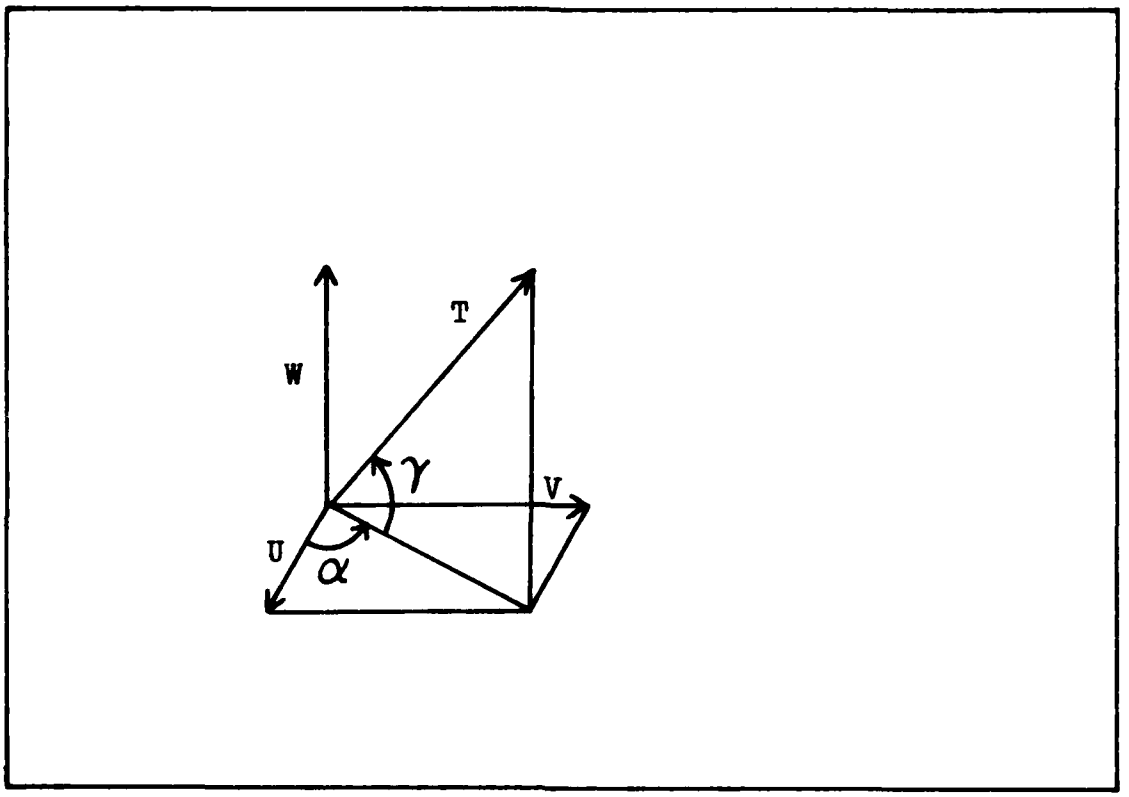

Fig 2. Acceleration Components

where

$$\gamma = \gamma(f) \tag{30}$$

$$\alpha = \alpha(f) \tag{31}$$

Substitution yields

$$\Delta\Omega = \frac{T\, a^2}{\mu \sin i} \int_0^g \sin\gamma \, \sin(f+s)\, df \tag{32}$$

$$\Delta i = \frac{T\, a^2}{\mu} \int_0^g \sin\gamma \, \cos(f+s)\, df \tag{33}$$

$$\Delta e = \frac{T\, a^2}{\mu}\int_0^g (\cos\gamma\, \cos\alpha \sin f + 2\cos\gamma \sin\alpha \cos f)\, df \qquad (34)$$

$$\Delta a = \frac{2\, T\, a^3}{\mu}\int_0^g \cos\gamma \sin\alpha \; df \qquad (35)$$

To find the optimum thrust history for one orbit, the approach used is to maximize Δi for a given Δa, subject to the additional constraint that $\Delta e = 0$. The performance index with constraint relationships is

$$J(\alpha,\gamma) = \int_0^g \frac{T\, a^2}{\mu} \sin\gamma \cos(f+s)\, df + \lambda_1\left[\int_0^g \frac{2\, T\, a^3}{\mu}\cos\gamma \sin\alpha \; df - \Delta a\right] + \lambda_2\int_0^g \frac{T\, a^2}{\mu}(\cos\gamma \cos\alpha \sin f + 2\cos\gamma \sin\alpha \cos f)\, df \qquad (36)$$

where λ_1 and λ_2 are Lagrange multipliers. Simplifying,

$$J(\alpha,\gamma) = \int_0^{\theta} \left[\frac{T\, a^2}{\mu} \left[\sin\gamma \cos(f+s) + \lambda_1\, a\, 2 \cos\gamma \sin\alpha \right.\right.$$

$$\left.\left. + \lambda_2(\cos\gamma \cos\alpha \sin f + 2 \cos\gamma \sin\alpha \cos f) \right] \right] df$$

$$- \lambda_1 \Delta a \qquad (37)$$

Call the integrand F for convenience. The calculus of variations can be used to show that the above functional has a stationary value when the following Euler equations are satisfied.[8]

$$\frac{\partial F}{\partial \alpha} - \frac{d}{df}\left[\frac{\partial F}{\partial \alpha'}\right] = 0 \qquad (38)$$

$$\frac{\partial F}{\partial \gamma} - \frac{d}{df}\left[\frac{\partial F}{\partial \gamma'}\right] = 0 \qquad (39)$$

where primes indicate the derivative with respect to the independent variable, f. Since α' and γ' do not occur in F, The Euler equations become algebraic equations rather than differential equations. Therefore, J has an extremal when

$$\frac{\partial F}{\partial \alpha} = 0 \qquad (40)$$

and

$$\frac{\partial F}{\partial \gamma} = 0 \qquad (41)$$

After performing the differentiation,

$$\frac{\partial F}{\partial \alpha} = \frac{\lambda_1 \, 2 \, T \, a^3}{\mu} \cos\gamma \, \cos\alpha$$

$$+\frac{\lambda_2 T \, a^2}{\mu}(2 \cos\gamma \, \cos\alpha \cos f - \cos\gamma \, \sin\alpha \sin f) \qquad (42)$$

$$\frac{\partial F}{\partial \gamma} = \frac{T \, a^2}{\mu}\cos\gamma \, \cos(f+s) - \frac{\lambda_1 2 \, T \, a^3}{\mu}\sin\gamma \, \sin\alpha$$

$$-\frac{\lambda_2 T \, a^2}{\mu}(\sin\gamma \, \cos\alpha \sin f + 2 \sin\gamma \, \sin\alpha \cos f) \qquad (43)$$

Substituting Eqs (42) and (43) into Eqs (40) and (41) and then simplifying gives

$$\tan\alpha = \frac{2(\lambda_1 a + \lambda_2 \cos f)}{\lambda_2 \sin f} \qquad (44)$$

$$\tan\gamma = \frac{\cos(f+s)}{\left[\lambda_2^2 \sin^2 f + 4(\lambda_1 a + \lambda_2 \cos f)^2\right]^{\frac{1}{2}}} \qquad (45)$$

Therefore, the optimal control law becomes

$$\alpha = \tan^{-1}\left[\frac{2(\lambda_1 a + \lambda_2 \cos f)}{\lambda_2 \sin f}\right] \tag{46}$$

$$\gamma = \tan^{-1}\left[\frac{\cos(f+s)}{\left[\lambda_2^2 \sin^2 f + 4(\lambda_1 a + \lambda_2 \cos f)^2\right]^{\frac{1}{2}}}\right] \tag{47}$$

Substitution of Eqs (46) and (47) into Eqs (32) through (35) gives

$$\Delta\Omega = \frac{T\, a^2}{\mu \sin i}\int_0^g \frac{\sin(f+s)\cos(f+s)\, df}{\left[\lambda_2^2\sin^2 f + 4(\lambda_1 a + \lambda_2 \cos f)^2 + \cos^2(f+s)\right]^{\frac{1}{2}}} \tag{48}$$

$$\Delta i = \frac{T\, a^2}{\mu}\int_0^g \frac{\cos^2(f+s)\, df}{\left[\lambda_2^2\sin^2 f + 4(\lambda_1 a + \lambda_2 \cos f)^2 + \cos^2(f+s)\right]^{\frac{1}{2}}} \tag{49}$$

$$\Delta e = \frac{T\, a^2}{\mu}\int_0^g \frac{\left[\lambda_2 \sin^2 f + 4\cos f\,(\lambda_1 a + \lambda_2 \cos f)\right] df}{\left[\lambda_2^2\sin^2 f + 4(\lambda_1 a + \lambda_2 \cos f)^2 + \cos^2(f+s)\right]^{\frac{1}{2}}} \tag{50}$$

$$\Delta a = \frac{4\, T\, a^3}{\mu}\int_0^g \frac{(\lambda_1 a + \lambda_2 \cos f)\, df}{\left[\lambda_2^2\sin^2 f + 4(\lambda_1 a + \lambda_2 \cos f)^2 + \cos^2(f+s)\right]^{\frac{1}{2}}} \tag{51}$$

The two constraint relationships, $\Delta e = 0$ and Δa as given, can be used to solve for the two Lagrange multipliers, λ_1 and λ_2. But these equations must be solved numerically. Before they can be solved numerically, however, s must be determined.

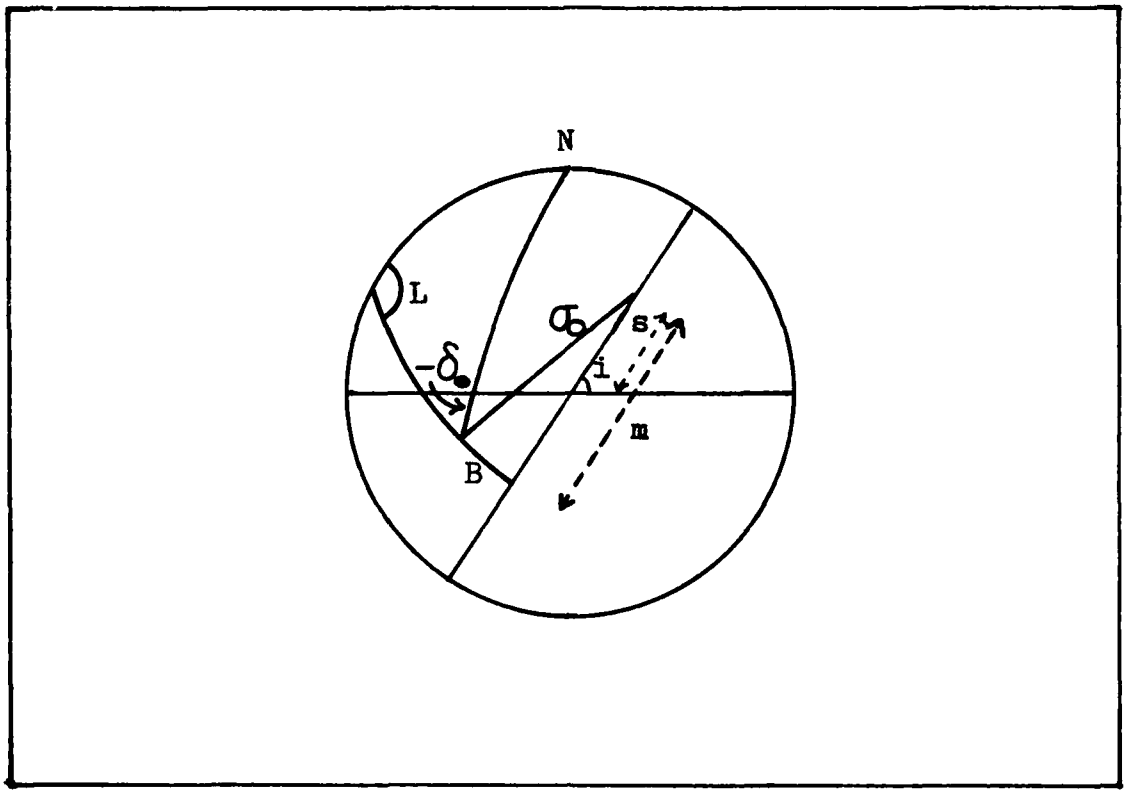

Fig 3. Sun-Orbit Geometrical Relationship

As mentioned earlier, s is a phase angle measured in the orbit plane between the ascending node and the point where the spacecraft exits the earth's shadow. Link[9] has derived the following expressions for the orbital coordinates of the anti-sun point to the orbital plane.

$$\sin B = -\sin\delta_\odot \cos i + \cos\delta_\odot \sin i \sin(\alpha_\odot - \Omega) \tag{52}$$

$$\sin L = -\cos(\alpha_\odot - \Omega)\frac{\cos\delta_\odot}{\cos B} \tag{53}$$

where B and L are angles as shown in Fig 3, $\alpha_\odot$ and $\delta_\odot$ are the right ascension and declination of the sun. The same reference also gives an expression for half the shadow

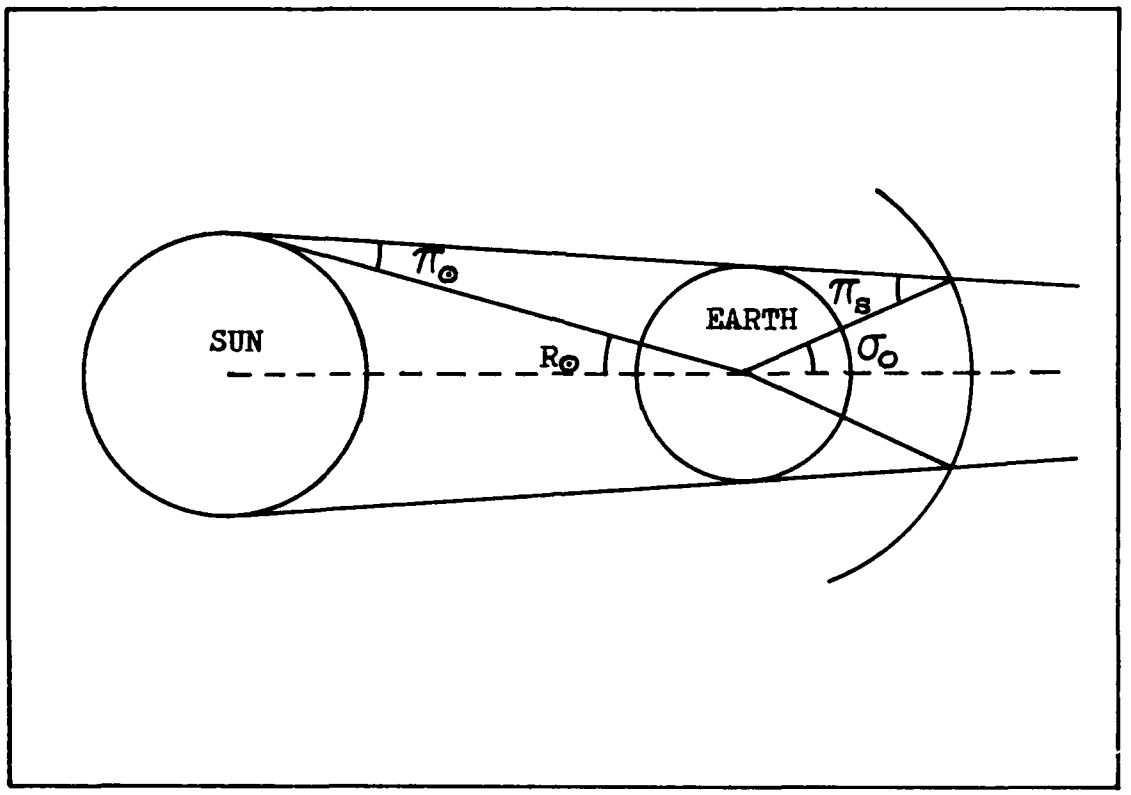

Fig 4. Shadow Geometry

angle, m:

$$\cos m = \frac{\cos \sigma_o}{\cos B} \tag{54}$$

where σ_o is half of the maximum shadow possible for a given altitude.

$$\sigma_o = \pi_\odot + \pi_s - R_\odot \tag{55}$$

where $\pi_\odot$ and π_s are the parallaxes of the sun and satellite respectively and R is the angular semi-diameter of the sun. See Figure 4. It can be seen in Figure 3 that

$$S = \frac{\pi}{2} - L + m \tag{5?}$$

When making the preceeding calculation, care must be exercised in choosing the proper quadrant for L. Once s is known, the upper limit of integration, g, can be found:

$$g = 2\pi - 2\,m = 2(\pi - m) \tag{57}$$

But first, for convenience, define

$$u = \lambda_1\, a \tag{58}$$

and

$$D = \lambda_2^2 \sin^2 f + 4(u + \lambda_2 \cos f)^2 + \cos^2(f+s) \tag{59}$$

Now the optimum control history for a single orbit can be found in the following manner. Given the orbital elements and the sun-earth geometrical relationship, s and g can be computed from Eqs (56) and (57). Then the two constraint relationships,

$$\int_0^g \frac{\lambda_2 \sin^2 f + 4 \cos f\,(u + \lambda_2 \cos f)\;\; df}{D^{\frac{1}{2}}} = 0 \tag{60}$$

and

$$\int_0^g \frac{2(u + \lambda_2 \cos f)\; df}{D^{\frac{1}{2}}} = \frac{\Delta a\, \mu}{2\, T\, a^3} \tag{61}$$

can be solved numerically to determine u and λ_2. These two values can then be substituted into the control law

which is repeated here;

$$\alpha = \tan^{-1}\left[\frac{2\,(u + \lambda_2 \cos f)}{\lambda_2 \sin f}\right] \tag{46}$$

$$\gamma = \tan^{-1}\left[\frac{\cos(f+s)}{\left[\lambda_2^2 \sin^2 f + 4(u + \lambda_2 \cos f)^2\right]^{\frac{1}{2}}}\right] \tag{47}$$

to find the control profile. This profile will maximize Δi for a given Δa, subject to $\Delta e = 0$.

Examples

Several examples are presented here to show the effects caused by various amounts of shadow and varying values of u. In all the examples, sun-earth relative geometry is assumed such that

$$s = \frac{3\pi}{2} + m \tag{62}$$

This value of s corresponds to the following conditions:

$a = 1.03$ DU $\qquad \alpha_\odot = 270^\circ$

$\Omega = 180^\circ \qquad \delta_\odot = -23.47^\circ$

These conditions would exist if the spacecraft were established in a 200 km parking orbit on the first day of winter.

Figure 5 shows the effect of shadow width on λ_2. Notice that when there is no shadow ($m = 0$), then $\lambda_2 = 0$. When $\lambda_2 = 0$, the constraint equation, $\Delta e = 0$, is not necessary.

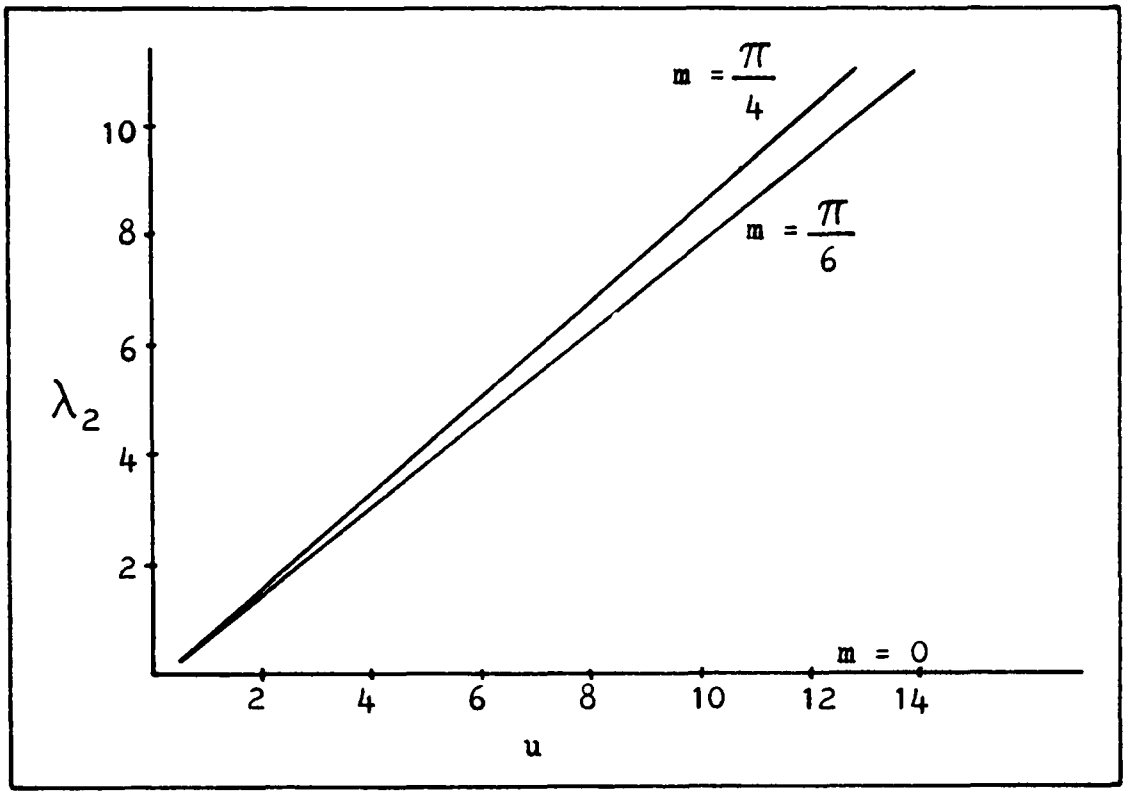

Fig 5. Shadow Effects on λ_2

Figure 6 shows the effect of shadow width on Δa and Δi. As would be expected, decreasing shadow width is accompanied by increasing Δa and Δi as a result of longer thrust application. Notice that $u = 0$ corresponds to inclination change only and that $u = \infty$ corresponds to semi-major axis change only. For computational purposes, $u = 100$ can be used for $u = \infty$, with good numerical accuracy. A plot of $\Delta\Omega$ versus u is not shown since $\Delta\Omega$ was very near zero for all cases that were examined. Also, since $\Delta\Omega$ was always at least three orders of magnitude less than Δa and Δi, its equation will be neglected in the remaining derivation.

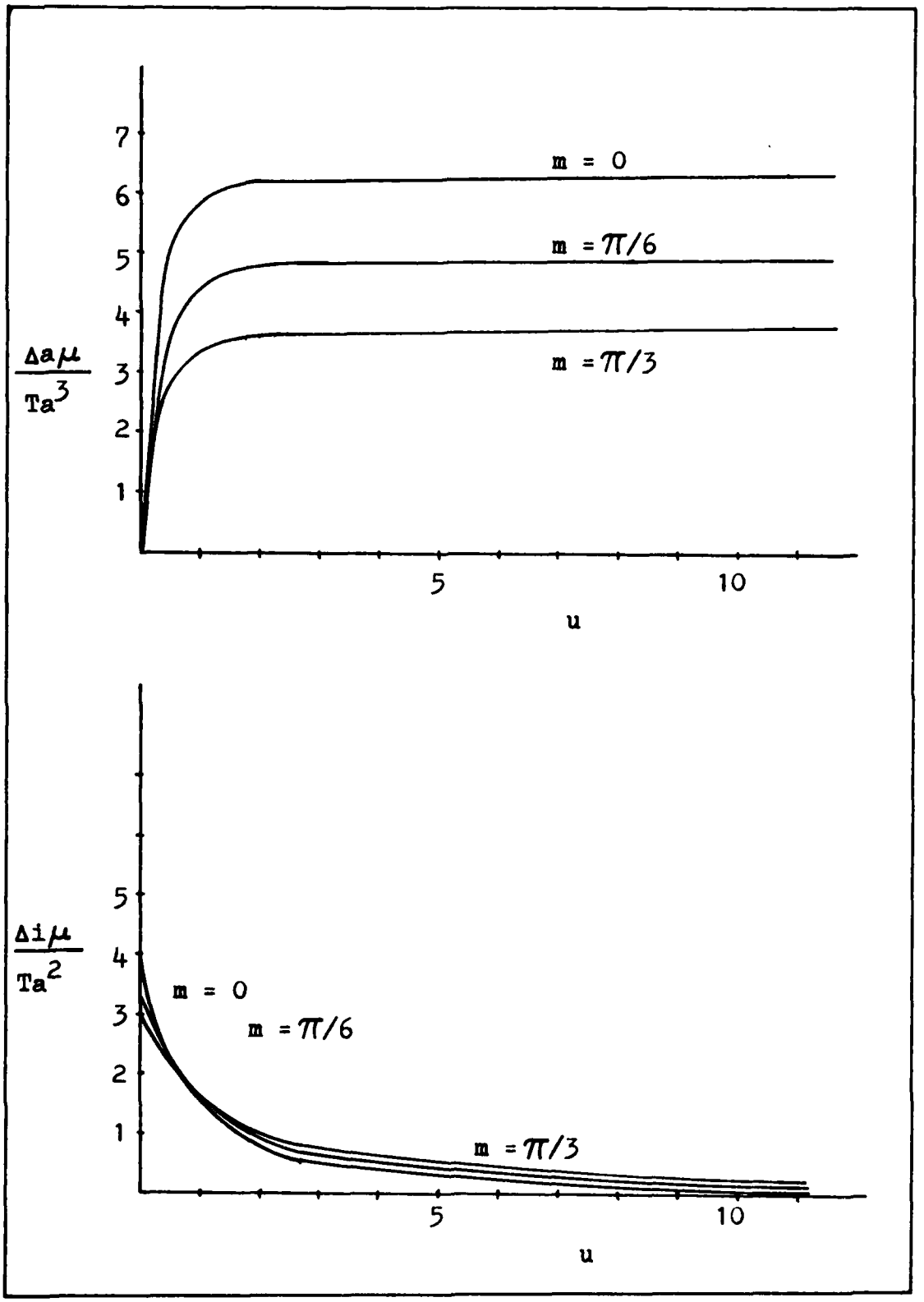

Fig 6. Shadow Effects on Δa and Δi

A comparison of the no shadow case and Alfano's results will help verify the derivation in this paper. As mentioned previously, when m = 0 , then $\lambda_2 = 0$. For $\lambda_2 = 0$, $\alpha = \pi/2$ and $\gamma = \tan^{-1}\left[\cos(f+s)/2u\right]$. These values correspond exactly with those presented in Alfano's paper. Additionally, consider using the control to cause semi-major axis change only. This case corresponds to $u = \infty$. By taking the limit as $u \rightarrow \infty$, it can be shown that $\Delta a \mu / T\, a^3 = 2\pi$. Finally, when only change in inclination is desired, $\Delta i \mu / T\, a^2 = 4$. Both of the last two results also agree exactly with those presented in Alfano's paper. Therefore, the control law is validated for the special case of no shadow.

Figures 7 through 9 show the effect of the control, u, for different values of m, the half-shadow angle. The γ curves appear as would be expected; for u = 0, all thrust is directed normal for the orbit plane; for greater values of u, less thrust is directed in the normal direction. The α curves may appear contradictory at first. As u increases, one would expect more thrust to be directed tangentially to achieve a greater Δa. But the figures indicate that greater values of u demand even greater divergence from pure tangential thrust ($\alpha = \pi/2$). Recall, however, that α only determines the direction of the thrust component in the orbit plane.

The magnitude of that component is T $\cos\gamma$. As u

increases, $\cos\gamma$ increases. So even though it appears that the tangential component decreases due to α, the coupling through the γ dependence insures that the tangential force is increasing. Of course, the increasing tangential acceleration requires more radial accelerations to maintain $\Delta e = 0$; thus causing it to appear that less tangential force is being applied.

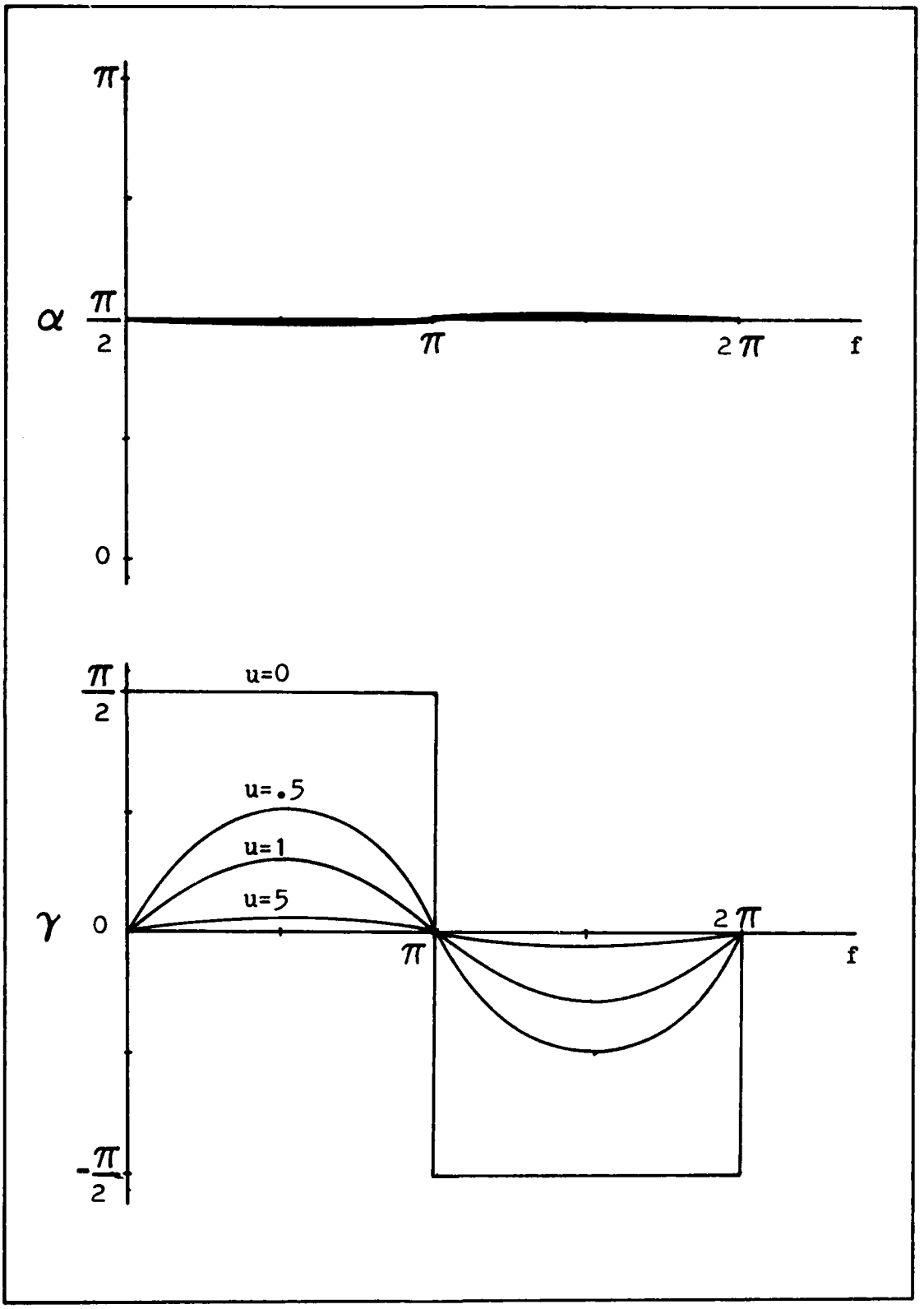

Fig 7. α and γ for m = 0

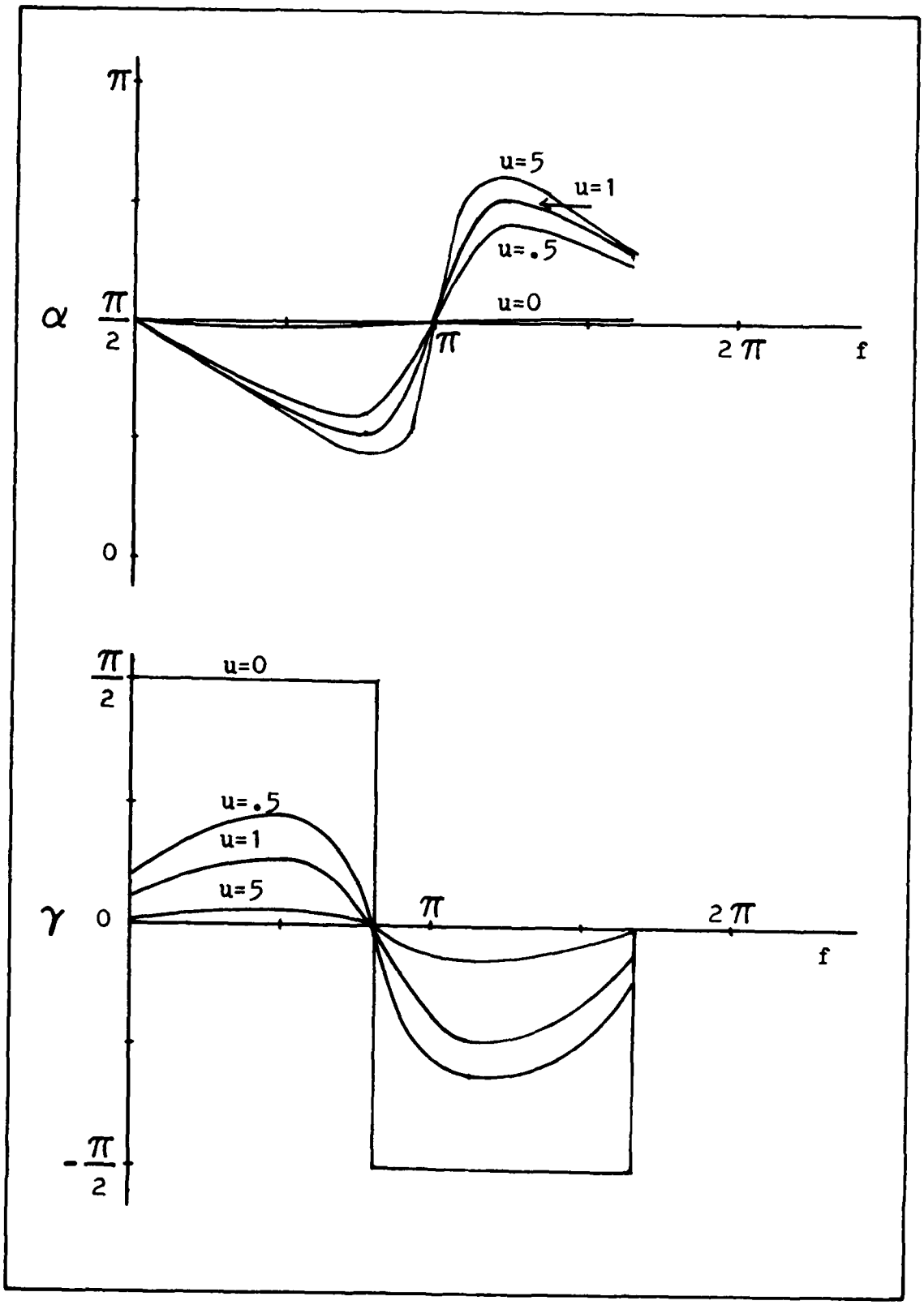

Fig 8. α and γ for m = $\pi/6$

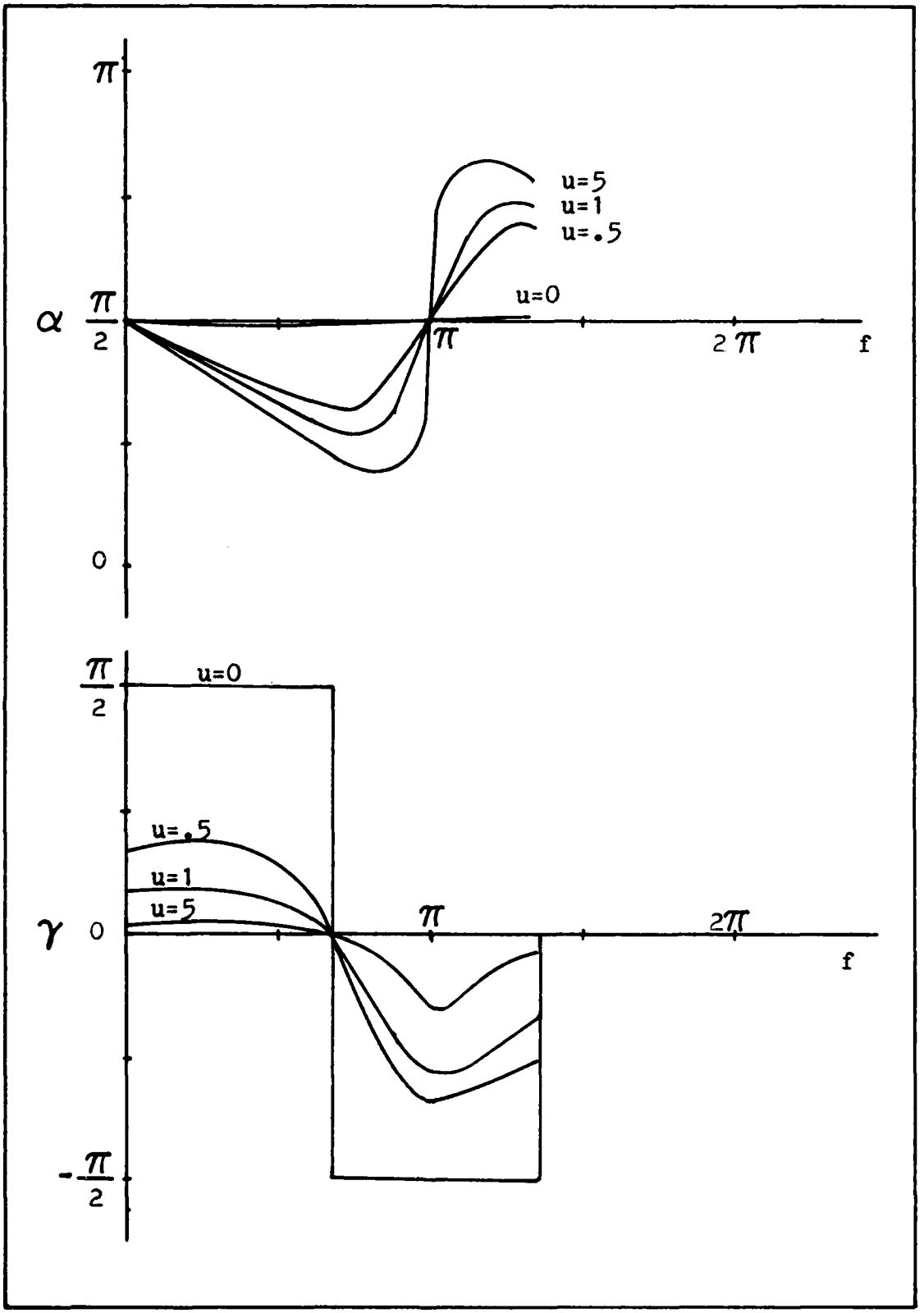

Fig 9. α and γ for m = $\pi/3$

III Slow Timescale Problem

Problem Statement

The purpose of solving the slow timescale problem is to determine how much to change semi-major axis and inclination on each orbit so that final boundary conditions are reached in minimum time. Fast timescale results are used to ensure optimal control during each orbit and to define the amount of change possible on a given orbit. Mass is recomputed for each orbit to compensate for propellant loss.

Derivation

Before the minimum time control problem can be solved, a few preliminary steps will be taken. An expression is needed for da/dt and di/dt for the slow timescale problem. Since the orbital elements change so little on each orbit, these rates can be approximated by

$$\frac{da}{dt} \simeq \frac{\Delta a}{\Delta t} \tag{63}$$

$$\frac{di}{dt} \simeq \frac{\Delta i}{\Delta t} \tag{64}$$

where Δt is the elapsed time for the particular orbit. For a circular orbit,

$$\Delta t = \mathcal{P} = 2\pi \left[\frac{a^3}{\mu}\right]^{\frac{1}{2}} \tag{65}$$

But the presence of shadow makes the above approximations

inaccurate. The elements a and i will only change when the spacecraft is in sunlight. Therefore, Δt must be adjusted to only cover that portion of the orbit when thrust is being applied.

$$\Delta t = \frac{g}{2\pi} TP = 2(\pi - m)\left[\frac{a^3}{\mu}\right]^{\frac{1}{2}} \tag{66}$$

Substitution yields

$$\frac{da}{dt} = \frac{2\,T\,a^{3/2}}{\mu^{\frac{1}{2}}(\pi - m)} \int_0^g \frac{(u + \lambda_2 \cos f)\, df}{D^{\frac{1}{2}}} \tag{67}$$

$$\frac{di}{dt} = \frac{T\,a^{\frac{1}{2}}}{2\mu^{\frac{1}{2}}(\pi - m)} \int_0^g \frac{\cos^2(f+s)\, df}{D^{\frac{1}{2}}} \tag{68}$$

Since the problem is to find a minimum thrusting time and hence minimum fuel, successive orbits will combine as if there were no coasting time through the shadow. The coasting time will be computed so the total transfer elapsed time will be known at the end.

As mentioned previously, corrections will be made for each orbit to compensate for increased acceleration caused by decreasing mass. For a constant thrust ion rocket, propellant flow is constant. Acceleration as a function of time can be modeled as

$$T(t) = \frac{T_0}{1 - \dot{m}_p t} \tag{69}$$

where T_0 is the initial vehicle acceleration, t is the time and $\dot{m}_p$ is the specific mass flow rate (mass flow rate divided by initial vehicle mass).

Since Eqs (67) and (68) can be solved more easily if there is no time dependence, a change of variable can be made. A new independent variable $\mathcal{T}$ can be defined such that

$$d\mathcal{T} = \left[\frac{T_0}{1 - \dot{m}_p t}\right] dt \tag{70}$$

Integrating, with $\mathcal{T} = 0$ when $t = 0$ yields

$$\mathcal{T} = -\frac{T}{\dot{m}_p} \ln (1 - \dot{m}_p t) \tag{71}$$

$\mathcal{T}$ is the total accumulated velocity change. Minimizing $\mathcal{T}$ will minimize thrusting time and fuel expended.

Converting from t to $\mathcal{T}$ gives

$$\frac{da}{d\mathcal{T}} = \frac{2\, a^{3/2}}{\mu^{\frac{1}{2}}(\pi - m)} \int_0^g \frac{(u + \lambda_2 \cos f)\, df}{D^{\frac{1}{2}}} \tag{72}$$

$$\frac{di}{d\mathcal{T}} = \frac{a^{\frac{1}{2}}}{\mu^{\frac{1}{2}} 2(\pi - m)} \int_0^g \frac{\cos^2(f+s)}{D^{\frac{1}{2}}} \tag{73}$$

Bryson and Ho[10] have shown that a minimum time solution satisfies the following conditions:

$$H(t_f) = 0 \tag{74}$$

$$\frac{\partial H}{\partial u_k} = 0 \qquad k = 1,2,3,\ldots,r \tag{75}$$

$$\lambda_j = \frac{\partial H}{\partial x_j} \qquad j = 1,2,3,\ldots,q \tag{76}$$

where H is the Hamiltonian, λ_j's are Lagrange multipliers, x_j's are the state variables, and the u_k's are the control variables. In this problem, $r = 1$ producing only one optimality condition and $q = 2$ because the simplified system has only two degrees of freedom. These equations will now be applied to this specific problem.

For this problem, the Hamiltonian is

$$H = \lambda_a \frac{da}{d\tau} + \lambda_i \frac{di}{d\tau} + 1 \tag{77}$$

Since t does not appear explicitly in H,

$$\dot{H} = 0 \tag{78}$$

Therefore, $H(t_f) = 0$ implies

$$H(t) = 0 \tag{79}$$

for all $t \geq 0$. So

$$\lambda_a \frac{da}{d\tau} + \lambda_i \frac{di}{d\tau} + 1 = 0 \tag{80}$$

for all time. Substitution produces

$$\lambda_a \left[\frac{2\, a^{3/2}}{\mu^{\frac{1}{2}}(\pi - m)} \int_0^g \frac{(u + \lambda_2 \cos f)\, df}{D^{\frac{1}{2}}} \right]$$

$$+ \lambda_i \left[\frac{a^{\frac{1}{2}}}{2\mu^{\frac{1}{2}}(\pi - m)} \int_0^g \frac{\cos^2(f+s)\, df}{D^{\frac{1}{2}}} \right] + 1 = 0 \qquad (81)$$

In this problem, Eq (75) becomes

$$\lambda_a \frac{\partial}{\partial u}\left[\frac{da}{d\tau}\right] + \lambda_i \frac{\partial}{\partial u}\left[\frac{di}{d\tau}\right] = 0 \qquad (82)$$

But

$$\frac{\partial}{\partial u}\frac{da}{d\tau} = \frac{2\, a^{3/2}}{\mu^{\frac{1}{2}}(\pi - m)} \int_0^g \frac{\left[\lambda_2^2 \sin^2 f + \cos^2(f+s)\right] df}{D^{3/2}} \qquad (83)$$

and

$$\frac{\partial}{\partial u}\frac{da}{d\tau} = \frac{-2\, a^{\frac{1}{2}}}{\mu^{\frac{1}{2}}(\pi - m)} \int_0^g \frac{(u + \lambda_2 \cos f)\cos^2(f+s)\, df}{D^{3/2}} \qquad (84)$$

Therefore,

$$\lambda_a \left[\frac{2\, a^{3/2}}{\mu^{\frac{1}{2}}(\pi - m)} \int_0^g \frac{\left[\lambda_2^2 \sin^2 f + \cos^2(f+s)\right]\, df}{D^{3/2}} \right]$$

$$- \lambda_i \left[\frac{2\, a^{\frac{1}{2}}}{\mu^{\frac{1}{2}}(\pi - m)} \int_0^g \frac{(u + \lambda_2 \cos f)\cos^2(f+s)\, df}{D^{3/2}} \right] = 0 \qquad (85)$$

For this problem, after the change of independent variable, Eq (76) becomes

$$\lambda_a' = - \frac{\partial H}{\partial a} \qquad (86)$$

$$\lambda_i' = - \frac{\partial H}{\partial i} \qquad (87)$$

where the prime indicates differentiation with respect to τ. Now

$$\frac{\partial H}{\partial a} = \lambda_a \frac{\partial}{\partial a}\left[\frac{da}{d\tau}\right] + \lambda_i \frac{\partial}{\partial a}\left[\frac{di}{d\tau}\right] \qquad (88)$$

But, remembering that s is a function of m and m is a function of both a and i,

$$\frac{\partial}{\partial a}\frac{da}{d\tau} = \left[\frac{\partial}{\partial a}\frac{da}{d\tau}\right] + \left[\frac{\partial}{\partial m}\frac{da}{d\tau}\right]\frac{\partial m}{\partial a} \qquad (89)$$

$$\frac{\partial}{\partial a}\frac{da}{d\tau} = \frac{3\,a^{\frac{1}{2}}}{\mu^{\frac{1}{2}}(\pi-m)}\int_0^g \frac{(u+\lambda_2\cos f)\,df}{D^{\frac{1}{2}}} \tag{90}$$

Since g is also a function of m

$$\frac{\partial}{\partial m}\frac{da}{d\tau} = \int_0^g \frac{\partial}{\partial m}\,\frac{2\,a^{3/2}(u+\lambda_2\cos f)\,df}{\mu^{\frac{1}{2}}(\pi-m)\,D^{\frac{1}{2}}}$$

$$+\left.\frac{2\,a^{3/2}(u+\lambda_2\cos f)}{\mu^{\frac{1}{2}}(\pi-m)\,D^{\frac{1}{2}}}\right|_g \frac{\partial g}{\partial m} \tag{91}$$

And, finally

$$\frac{\partial}{\partial m}\frac{da}{d\tau} = \frac{2\,a^{3/2}}{\mu^{\frac{1}{2}}(\pi-m)^2}\int_0^g \frac{(u+\lambda_2\cos f)\,df}{D^{\frac{1}{2}}}$$

$$+\frac{2\,a^{3/2}}{\mu^{\frac{1}{2}}(\pi-m)}\int_0^g \frac{(u+\lambda_2\cos f)\sin(f+s)\cos(f+s)\,df}{D^{3/2}}$$

$$-\frac{4\,a^{3/2}(u+\lambda_2\cos 2m)}{\mu^{\frac{1}{2}}(\pi-m)\left[\lambda_2^2\sin^2 2m+4(u+\lambda_2\cos 2m)^2+\cos^2(s-2m)\right]^{\frac{1}{2}}} \tag{92}$$

Now, to find $\partial m/\partial a$, recall Eqs (52), (54), and (55). Substitution of the appropriate physical constraints gives

$$\cos\sigma_o = \left[1-\frac{1}{a^2}\right]^{\frac{1}{2}} F_o + \frac{1}{a}\,G_o \tag{93}$$

where F_0 and G_0 are constants depending on the size of the earth and sun and the distance between them.

$$F_0 = .99994668 \qquad G_0 = .0046229536$$

Also,

$$\cos B = \left[1 - (\cos\delta_\odot \sin i \sin(\alpha_\odot - \Omega) - \sin\delta_\odot \cos i)^2\right]^{\frac{1}{2}} \tag{94}$$

$$\frac{\partial m}{\partial a} = \frac{\partial}{\partial a}\left[\cos^{-1}\left(\frac{\cos\sigma}{\cos B}\right)\right] \tag{95}$$

$$\frac{\partial m}{\partial a} = \frac{G_0 - \dfrac{F_0}{\left[a^2 - 1\right]^{\frac{1}{2}}}}{a^2\left[\cos^2 B - \cos^2\sigma_0\right]^{\frac{1}{2}}} \tag{96}$$

For convenience, let

$$X = \frac{\partial m}{\partial a} = \frac{G_0 - F_0(a^2-1)^{-\frac{1}{2}}}{a^2\left[\cos^2 B - \cos^2\sigma\right]^{\frac{1}{2}}} \tag{97}$$

Continuing to construct more terms of Eq (88),

$$\frac{\partial}{\partial a}\left[\frac{di}{d\tau}\right] = \left[\frac{\partial}{\partial a}\frac{di}{d\tau}\right] + \left[\frac{\partial}{\partial m}\frac{di}{d\tau}\right]\frac{\partial m}{\partial a} \tag{98}$$

$$\frac{\partial}{\partial a}\frac{di}{d\tau} = \frac{1}{4\mu^{\frac{1}{2}}a^{\frac{1}{2}}(\pi-m)}\int_0^g \frac{\cos^2(f+s)\ df}{D^{\frac{1}{2}}} \tag{99}$$

$$\frac{\partial}{\partial m}\frac{di}{d\tau} = \frac{-a^{\frac{1}{2}}}{\mu^{\frac{1}{2}}(\pi-m)}\int_0^g \frac{\sin(f+s)\ \cos(f+s)\ df}{D^{\frac{1}{2}}}$$

$$+ \frac{a^{\frac{1}{2}}}{2\mu^{\frac{1}{2}}(\pi-m)^2}\int_0^g \frac{\cos^2(f+s)\ df}{D^{\frac{1}{2}}}$$

$$+ \frac{a^{\frac{1}{2}}}{2\mu^{\frac{1}{2}}(\pi-m)}\int_0^g \frac{\sin(f+s)\ \cos^3(f+s)\ df}{D^{3/2}}$$

$$- \frac{a^{\frac{1}{2}}\cos^2(s-2m)}{\mu^{\frac{1}{2}}(\pi-m)\ \left[\lambda_2^2\sin^2 2m+4(u+\lambda_2\cos 2m)^2+\cos^2(s-2m)\right]^{\frac{1}{2}}} \tag{100}$$

Substituting Eqs (90), (92), (97), (99) and (100) into Eq (86) yields

$$\lambda_a' = -\lambda_a \left[\frac{a^{\frac{1}{2}}\left[3(\pi-m)+2 X a\right]}{\mu^{\frac{1}{2}}(\pi-m)^2} \int_0^g \frac{(u+\lambda_2 \cos f)\, df}{D^{\frac{1}{2}}} \right.$$

$$+ \frac{2 X a^{3/2}}{\mu^{\frac{1}{2}}(\pi-m)} \int_0^g \frac{(u+\lambda_2 \cos f)\sin(f+s)\cos(f+s)\, df}{D^{3/2}}$$

$$\left. - \frac{4 X a^{3/2}(u+\lambda_2 \cos 2m)}{\mu^{\frac{1}{2}}(\pi-m)\left[\lambda_2^2 \sin^2 2m + 4(u+\lambda_2 \cos 2m)^2 + \cos^2(s-2m)\right]^{\frac{1}{2}}} \right]$$

$$-\lambda_i \left[\frac{(\pi-m)+2 X a}{4\mu^{\frac{1}{2}} a^{\frac{1}{2}}(\pi-m)^2} \int_0^g \frac{\cos^2(f+s)\, df}{D^{\frac{1}{2}}} \right.$$

$$- \frac{X a^{\frac{1}{2}}}{\mu^{\frac{1}{2}}(\pi-m)} \int_0^g \frac{\sin(f+s)\cos(f+s)\, df}{D^{\frac{1}{2}}}$$

$$+ \frac{X a^{\frac{1}{2}}}{\mu^{\frac{1}{2}}(\pi-m)} \int_0^g \frac{\sin(f+s)\cos(f+s)\, df}{D^{3/2}}$$

$$\left. - \frac{X a^{\frac{1}{2}} \cos^2(s-2m)}{\mu^{\frac{1}{2}}(\pi-m)\left[\lambda_2^2 \sin^2 2m + 4(u+\lambda_2 \cos 2m)^2 + \cos^2(s-2m)\right]^{\frac{1}{2}}} \right] \qquad (101)$$

In a similar manner, λ_i' can be found to be

$$\lambda_i' = -\lambda_a \left[\frac{2\,Y\,a^{3/2}}{\mu^{\frac{1}{2}}(\pi-m)^2} \int_0^g \frac{(u+\lambda_2 \cos f)\,df}{D^{\frac{1}{2}}} \right.$$

$$+ \frac{2\,Y\,a^{3/2}}{\mu^{\frac{1}{2}}(\pi-m)} \int_0^g \frac{(u+\lambda_2 \cos f)\,\sin(f+s)\,\cos(f+s)\,df}{D^{3/2}}$$

$$\left. - \frac{4\,Y\,a^{3/2}\,(u+\lambda_2 \cos 2m)}{\mu^{\frac{1}{2}}(\pi-m)\left[\lambda_2^2 \sin^2 2m + 4(u+\lambda_2 \cos 2m)^2 + \cos^2(s-2m)\right]^{\frac{1}{2}}} \right]$$

$$- i \left[\frac{-Y\,a^{\frac{1}{2}}}{\mu^{\frac{1}{2}}(\pi-m)} \int_0^b \frac{\sin(f+s)\,\cos(f+s)\,df}{D^{\frac{1}{2}}} \right.$$

$$+ \frac{Y\,a^{\frac{1}{2}}}{2\mu^{\frac{1}{2}}(\pi-m)^2} \int_0^g \frac{\cos^2(f+s)\,df}{D^{\frac{1}{2}}}$$

$$+ \frac{Y\,a^{\frac{1}{2}}}{2\mu^{\frac{1}{2}}(\pi-m)} \int_0^g \frac{\sin(f+s)\,\cos^3(f+s)\,df}{D^{3/2}}$$

$$\left. - \frac{Y\,a^{\frac{1}{2}}\,\cos^2(s-2m)}{\mu^{\frac{1}{2}}(\pi-m)\left[\lambda_2^2 \sin^2 2m + 4(u+\lambda_2 \cos 2m)^2 + \cos^2(s-2m)\right]^{\frac{1}{2}}} \right] \quad (102)$$

where

$$Y = \frac{\partial m}{\partial i} = \frac{-\cos\sigma_0 \sin B \cos(\delta_0 - i)}{\cos^2 B \left[\cos^2 B - \cos^2\sigma_0\right]^{\frac{1}{2}}} \quad (103)$$

Now, Eqs (81) and (85) can be solved simultaneously for λ_a and λ_i in terms of integrals containing the state and control variables. From Eq (85),

$$\lambda_i = \frac{\lambda_a \, a \int_0^g \frac{\left[\lambda_2^2 \sin^2 f + \cos^2(f+s)\right] \, df}{D^{3/2}}}{\int_0^g \frac{(u + \lambda_2 \cos f) \cos^2(f+s) \, df}{D^{3/2}}} \tag{104}$$

Substituting this result into Eq (81) gives

$$a = \left[\frac{1}{Q(u,s)}\right] \frac{2\mu^{\frac{1}{2}}(\pi - m)}{a^{3/2}} \int_0^g \frac{(u + \lambda_2 \cos f) \cos^2(f+s) \, df}{D^{3/2}} \tag{105}$$

where

$$Q(u,s) = \int_0^g \frac{4(u + \lambda_2 \cos f) \, df}{D^{\frac{1}{2}}} \int_0^g \frac{(u + \lambda_2 \cos f) \cos^2(f+s) \, df}{D^{3/2}}$$

$$+ \int_0^g \frac{\cos^2(f+s) \, df}{D^{\frac{1}{2}}} \int_0^g \frac{\left[\lambda_2^2 \sin^2 f + \cos^2(f+s)\right] \, df}{D^{3/2}} \tag{106}$$

These two equations can be substituted into either equation (101) or (102) to also produce an integral equation in terms of the state and control variables. Now, using the new expression for Eqs (101) or (102), and the two state Eqs (72) and (73), the minimum time problem can be solved.

There are three equations and three unknowns: a, i, and u. Solving these equations is not a trivial task, however. Implementation of this solution is described in the following section.

Implementation

The minimum time profile is determined in the following manner. Choose Eq (101) or (102) to use. To demonstrate, use Eq (101). Pick a starting value for λ_a. Given this $\lambda_a(0)$, Eq (105) can be solved numerically to determine what u would produce that λ_a. Remember that selecting or finding u also determines λ_2 as a result of satisfying the constraint $\Delta e = 0$. Now these values of u and λ_2 are used in the state Eqs (72) and (73) to find Δa and Δi. Also, a, i and m are used to compute Δt and ΔT. This ΔT is used to find the new λ_a. λ_a is then used to repeat the process until final boundary conditions are met. If final boundary conditions are not met, a new $\lambda_a(0)$ is chosen. This process continues until a $\lambda_a(0)$ is found which causes the final boundary conditions to be achieved. Then u will be determined for the entire profile.

Although this method of solution may sound rather straight forward, there can be some major problems. At first glance, it would appear that one should choose the λ_i equation to use. That equation has fewer terms and Y as a factor in all its terms. Recall that Y is the partial of m with respect to i. When $m = 0$, $Y = 0$ and

$$\lambda_i' = 0 \tag{107}$$

Therefore

$$\lambda_i = \text{constant} \tag{108}$$

It was found by experience, however, that in the range of interest for values of λ_i, u is double-valued. It was also found that λ_i varied dramatically for different values of a and i. See figures 10 and 11. Figure 10 shows λ_a and λ_i versus u for a = 1.03 DU's and i = .4974 radians. Figure 11 shows the same functions for a = 6.6 DU's (geosynchronous) and i = 0. Notice that the λ_a curve maintains its shape and only changes slightly. The λ_i curve, however, is not as well behaved. The peak on that curve shifts upward and to the right. Using λ_i, the optimal profile attempts to move from the right side of the peak to the left. Numerical search schemes in the vicinity of the zero slope diverged and therefore an optimal profile could not be found.

By using the λ_a equation, an optimal profile could be found as long as large values of u are not encountered. This would occur if the starting λ_a was chosen where the λ_a curve was nearly horizontal. Fortunately, that region corresponds to transfers which will be shown to not be optimal.

The second major problem in implementing this solution is developing a search scheme to find the correct

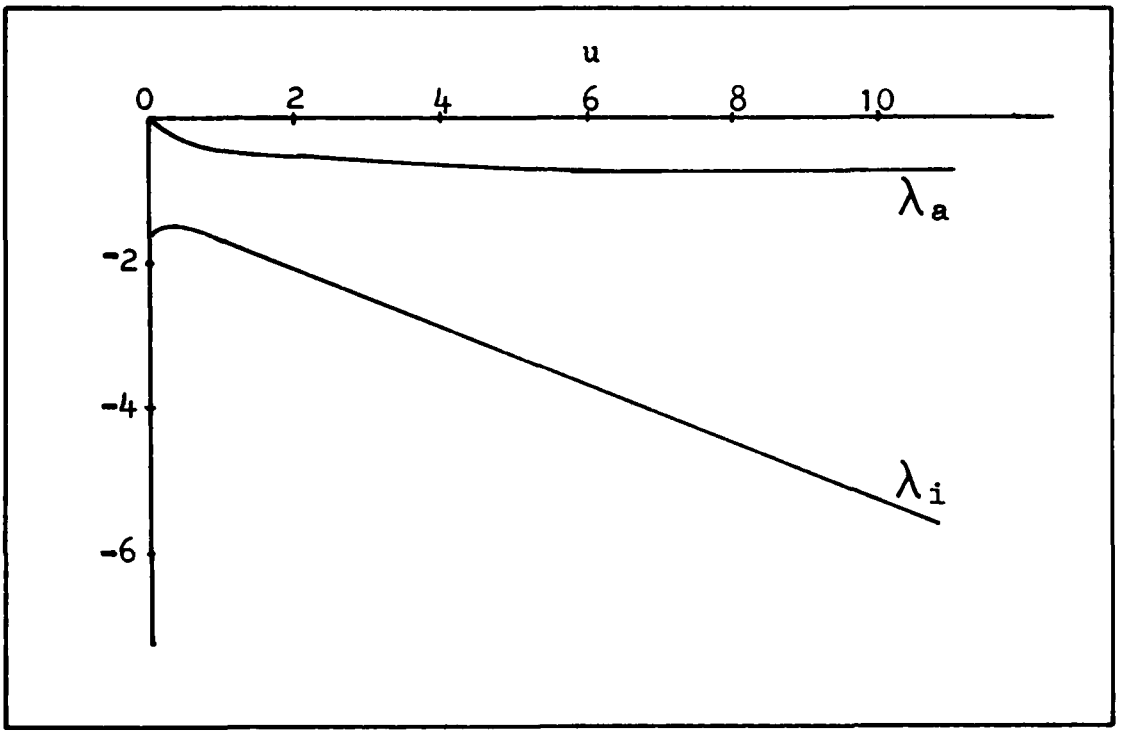

Fig 10. λ_a and λ_i for Initial Conditions

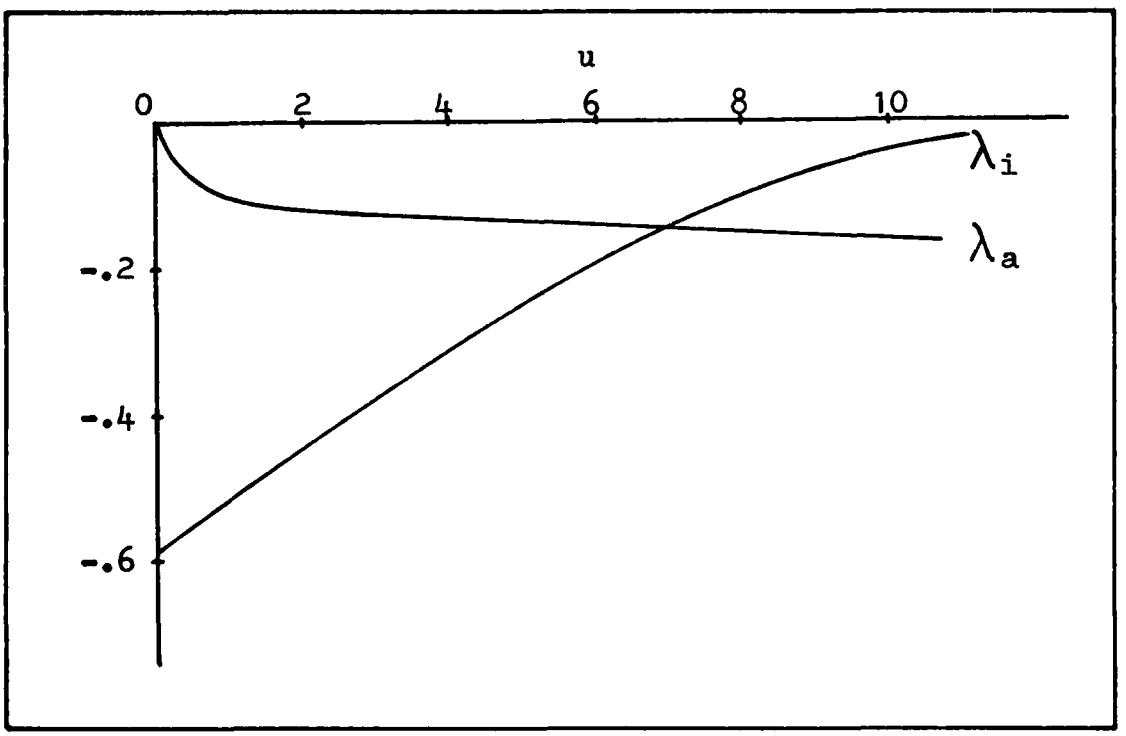

Fig 11. λ_a and λ_i for Final Conditions

$\lambda_a(0)$. For all cases considered in this paper, choosing a $\lambda_a(0)$ near zero caused i_f to be reached before a_f. For $\lambda_a(0)$ in the horizontal portion of its graph, a_f was reached first. The optimum choice of $\lambda_a(0)$ for a minimum time solution occurs somewhere between these other values. Unfortunately, more than one local minimum may exist in this region. In the next chapter, it will be shown that this does not appear to be a serious problem for the particular transfers that were considered. When more than one minimum occured, the transfer times were very close to one another.

In summary, the method outlined in the chapter can be used to solve the minimum time transfer problem. The solution may only be a local minimum, however.

IV Results

The equations derived in the preceeding chapters were applied to three specific transfers. One transfer did not involve any time in shadow; another caused the spacecraft to be in shadow for about half its orbits; and the last transfer required shadow penetration during about 95% of its orbits. All three transfers required the same semi-major axis and inclination change. For all, a_i corresponded to a parking orbit altitude of 200 km and a_f corresponded to geo-synchronous altitude. Beginning and ending inclinations were chosen to cause the varying amounts of shadow time. In all three cases,

$$\alpha_\odot = 270^\circ \qquad \Omega = 180^\circ \qquad \delta_\odot = -23.47^\circ$$

Also, to aid comparison, Alfano's values for specific impulse (5000 sec) and specific mass flow rate (2.0×10^{-7}/sec) were used. Figures 12 through 14 show how a, i and shadow angle vary during each of the three profiles.

Case I

This case was the transfer that did not penetrate the earth's shadow at any time. This case was designed primarily to validate the slow timescale solution by comparing it with Alfano's results for the identical transfer. Using the solution presented here, the total accumulated velocity change ($\mathcal{T}$) was only 2.7% greater than Alfano's. The difference was caused primarily by numerical problems associated with finding λ_2 from the constraint relationship, $\Delta e = 0$.

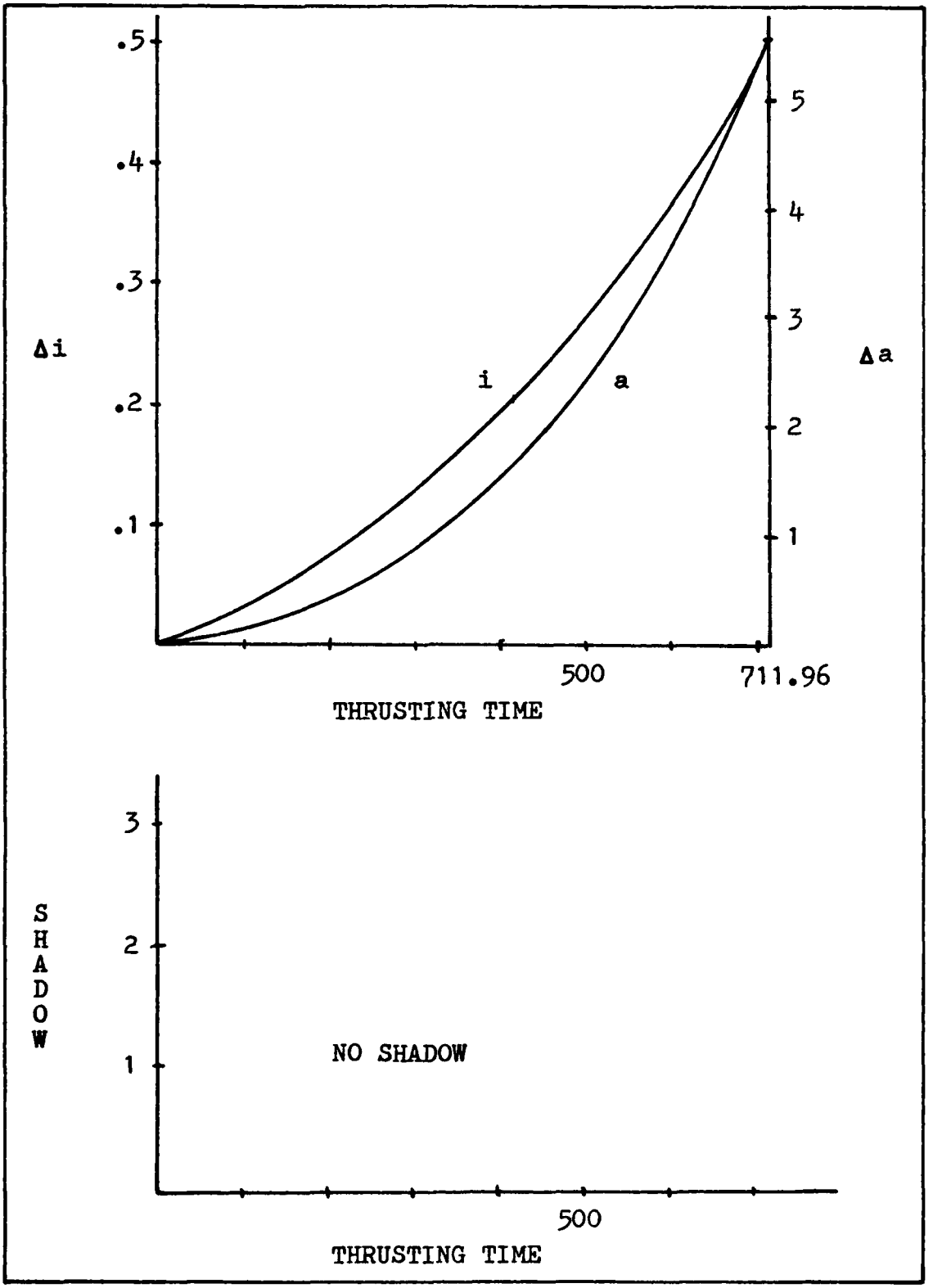
.5
.4
.3
.2
.1
Δi
i
a
5
4
3
2
1
Δa
500
711.96
THRUSTING TIME
3
2
1
SHADOW
NO SHADOW
500
THRUSTING TIME

Fig 12. CASE I

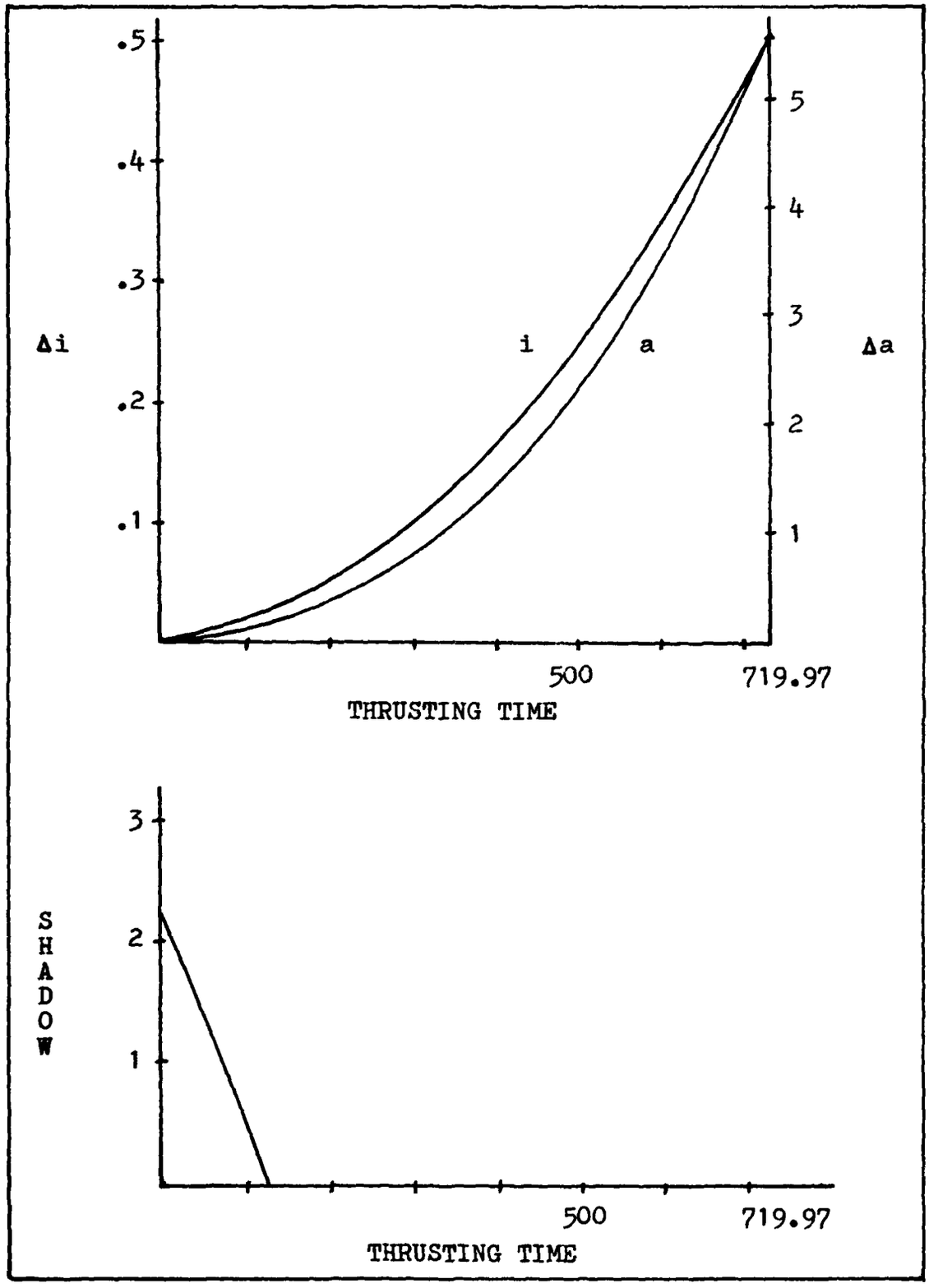

Fig 13. CASE II

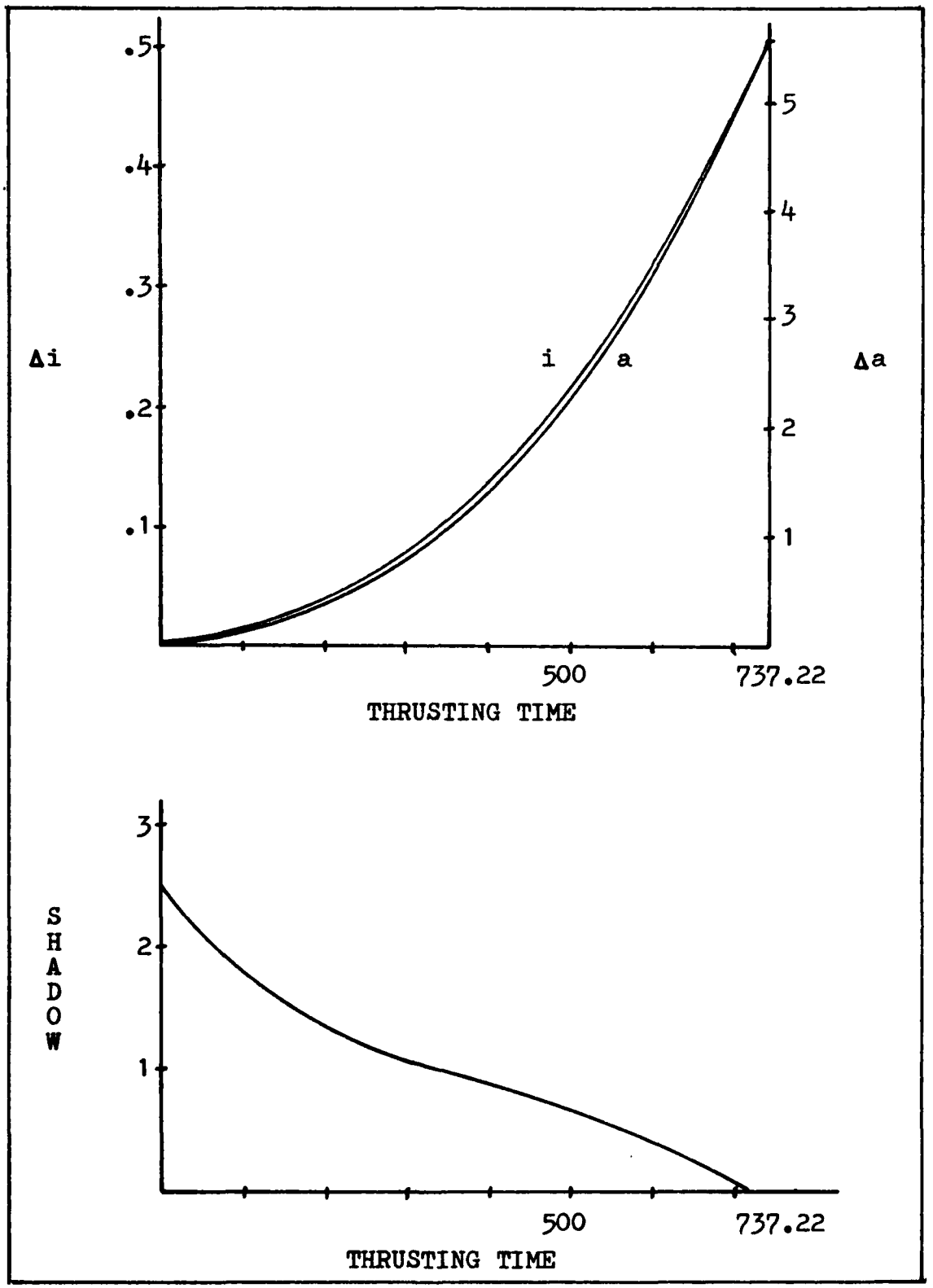

Fig 14. CASE III

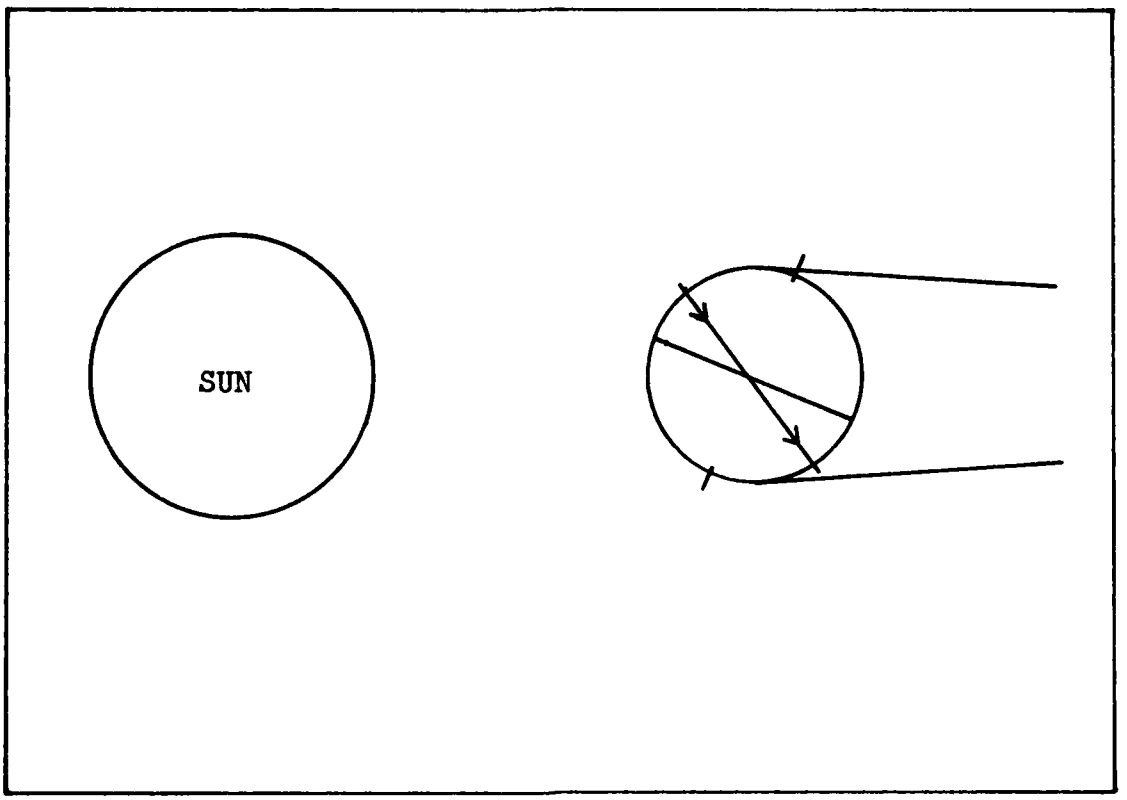

Fig 15. Case II Initial Conditions

Although λ_2 should equal zero when there is no shadow, λ_2 was always found to be very near zero. Consequently, a small amount of radial thrust was applied throughout the transfer making it less efficient. A more accurate search routine for λ_2 should reduce or eliminate the difference. For this reason, it is believed that this solution is validated.

Case II

The geometry for this case is shown in Figure 15. The initial conditions would occur with a noon launch out of Cape Canaveral on the first day of winter. In this transfer, the spacecraft experiences an eclipse on each of its first 20 orbits.

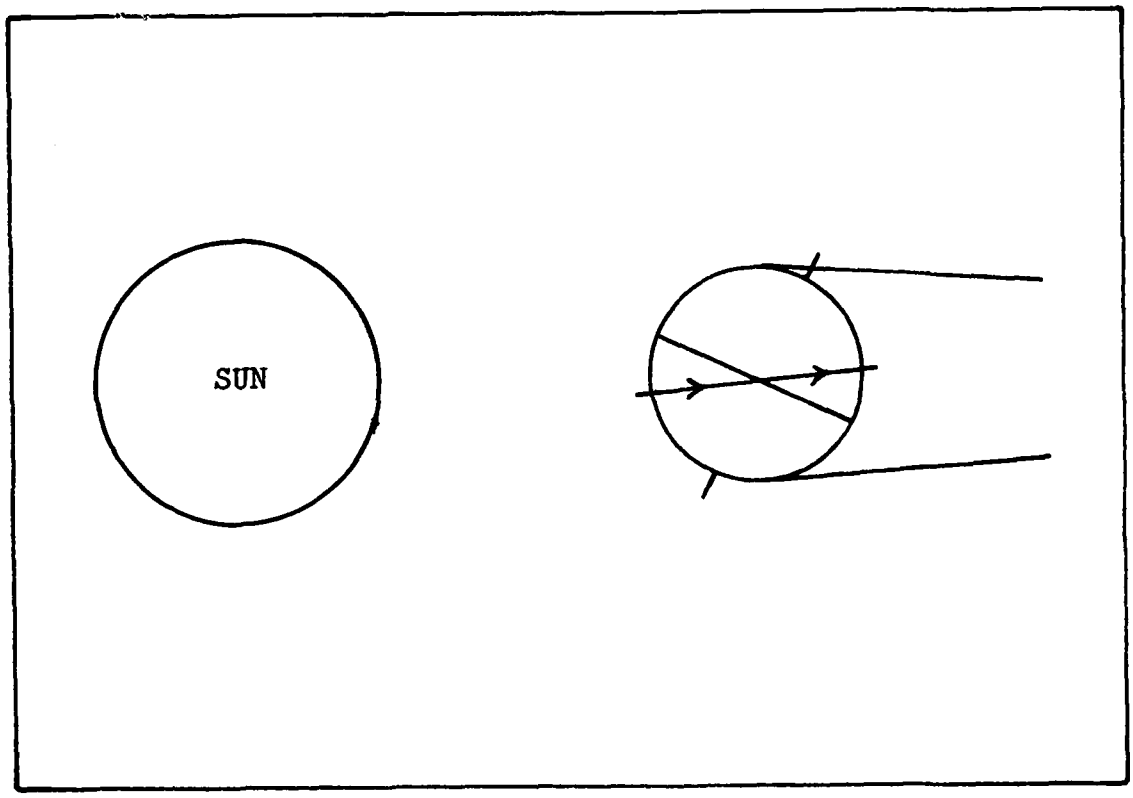

Fig 16. Case III Initial Conditions

For this transfer, T was only 1.17% greater than the case with no shadow. This small amount represents the penalty associated with maintaining $\Delta e = 0$ during the orbits when the shadow is penetrated. Even the total transfer time including coasting periods is only 40 TU's or 5.62% longer.

Case III

The initial geometry for this transfer is shown on Figure 16. These conditions would occur with a midnight launch on the first day of winter. This transfer was chosen because it required the spacecraft to penetrate the shadow for many orbits. As expected, this transfer required more fuel and time. There is a 3.76% increase in T. The total

time experienced a large 24.8% increase, however. Again, this is not surprising, since the spacecraft had many more coasting periods.

Multiple Local Minima

As previously discussed, several minima may exist. Using Case II as an example, it was found that at least two local minima did exist. For $\lambda_a(0) = -.69023$, T and thrusting time were as described previously and shown in Figure 12. For $\lambda_a(0) = -.73123$, T was only .001 greater. The two profiles were slightly different. In the second profile, semi-major axis changed more rapidly at first causing shadow exit one orbit earlier.

The presence of multiple minima is not really a problem, however. A reasonable step size for $\lambda_a(0)$ of .01 identified where the minima could be found. Also, it was noted that there is a specific range of $\lambda_a(0)$ where these minima seem to occur. If $\lambda_a(0)$ is such that i_f is reached first, and, if thrust is used after that point to change a only, then the amount of time needed to reach a_f is an indication of whether a minimum can exist in a neighborhood of that $\lambda_a(0)$. If a_f cannot be reached within one orbit, then $\lambda_a(0)$ does not appear to be near a minimum. A plot of T versus $\lambda_a(0)$ seems to be steadily decreasing in this region; see Figure 17. The same argument can be made for $\lambda_a(0)$'s where a_f is reached first. If i_f cannot be reached within one orbit using only thrust

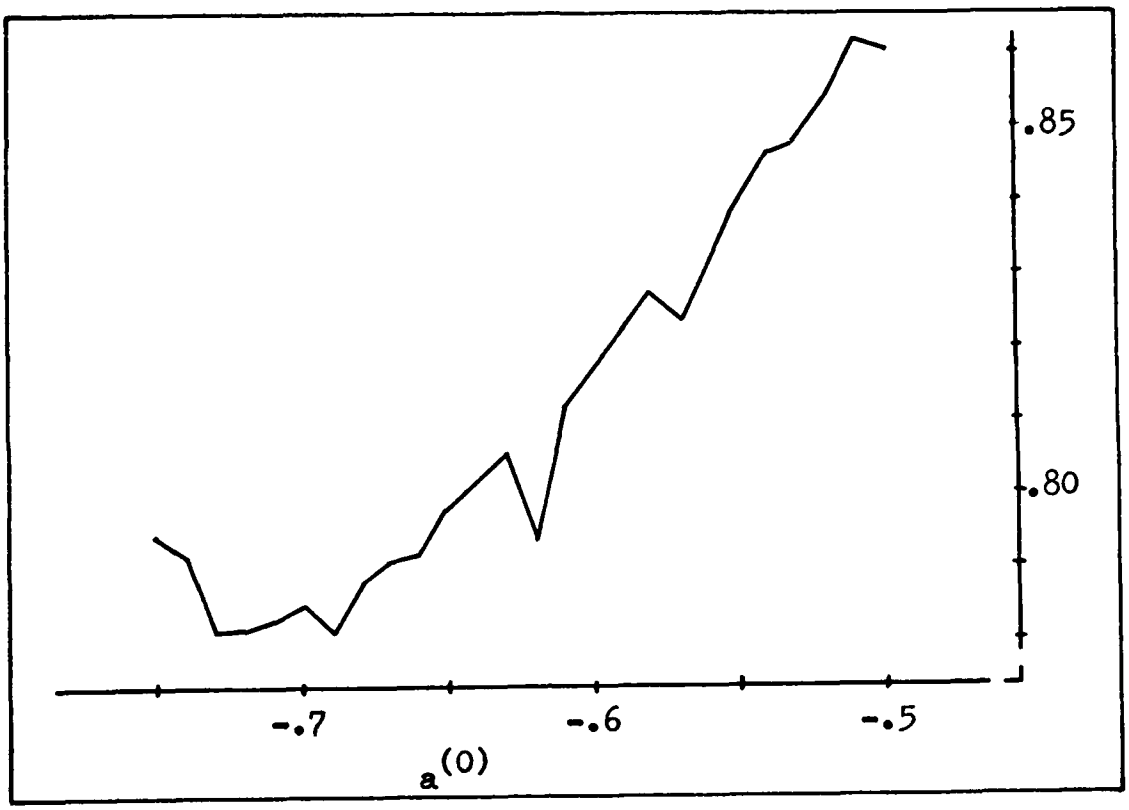

Fig 17. $\mathcal{T}$ versus $\lambda_a(0)$

normal to the plane, then a minimum does not apparently exist in that region. Again, $\mathcal{T}$ seems to be steadily increasing in this area. In either case, if the other boundary condition can be reached within one orbit, then a minimum is nearby. Also, the new $\lambda_a(0)$ should be greater if i_f was reached first and less if a_f was achieved first. Knowing these characteristics makes it relatively easy to find the minima.

General Observations

There are two additional characteristics of these transfers that bear mentioning. Several other initial conditions were used to examine certain characteristics.

Full transfers were not accomplished, but two trends did appear.

The first trend to note is that in no case did the control law direct an inclination change away from i_f. It was thought that the minimum time solution may require a Δi away from i_f to reduce shadow time. Apparently, the cost of moving away from the final boundary condition is more than the benefit gained from reducing the shadow.

The other trend that was noticed was that the control, u, increases until the shadow is less than approximately 2.1 radians. If the shadow is less than that amount, u decreases. The value at which this occurs is not constant for all the transfers, but it is near 2.1 radians.

It should also be pointed out that these trends were not contradicted in any of these trials.

V. Conclusions and Recommendations

A minimum time, minimum fuel control law for a vehicle using discontinuous low thrust has been presented. This control is optimal, subject to the constraint that $\Delta e = 0$.

If vehicle design prevents continuous thrust application, there is only a small penalty over a design which allows continuous thrust. In particular, an ion rocket powered by solar panels would be competitive with one powered by nuclear power, even if the former could not operate in shadow. The reduction in weight and complexity by eliminating a nuclear power source may more than offset the weight of a small amount of additional fuel.

This solution assumed a spherical earth, as well as constant $\alpha_\odot$ and $\delta_\odot$. The oblateness of the earth would cause the line of nodes to regress. Additionally, the actual changes in $\alpha_\odot$ and $\delta_\odot$ will affect the size of the shadow. These two effects combine to make the length of the transfer highly dependent on the launch time and inclination. The proper selection of when to launch into which initial parking orbit can minimize the effect of shadow penetration.

This solution also assumed low thrust. If thrust is too great, this control law is invalid because Δa and Δi would not be small on each orbit.

A recommendation to further this study would be to find an optimum launch time to perform a given transfer. Another continuation would be to find the optimum control law without requiring $\Delta e = 0$.

Bibliography

1. NASA. Ion Propulsion For Spacecraft. Washington D.C.: U.S. Government Printing Office, 1977.

2. Alfano, Capt. Salvatore. Low Thrust Orbit Transfer. MS Thesis. School of Engineering, Air Force Institute of Technology (AU), Wright Patterson AFB OH, December 1982.

3. Moeckel, W. E. Trajectories With Constant Tangential Thrust in Central Gravitational Fields. NASA TR. Washington D. C. : U. S. Government Printing Office, 1960.

4. Ehricke, Kraft A. Space Flight, Volume 2: Dynamics. New York: McGraw - Hill Book Company, 1962.

5. Stuhlinger, Ernst. Ion Propulsion for Space Flight. New York: McGraw - Hill Book Company, 1964.

6. LaFleur, Joseph D., Jr. "Nuclear Power Systems for Spacecraft," IEEE Transactions on Aerospace and Electronic Systems, AES-6: 147-164 (March 1970).

7. Danby, J.M.A. Fundamentals of Celestial Mechanics. New York: MacMillan Publishing Co., Inc., 1962.

8. Gelfand, I.M. and Fomin, S.V. Calculus of Variations. Translated by Richard A. Silverman. New Jersey: Prentice - Hall, Inc., 1963.

9. Link, F. Eclipse Phenomena in Astronomy. New York: Springer - Verlag, Inc., 1969.

10. Bryson, A.E. and Ho, Y.C. Applied Optimal Control. Massachusetts: Ginn and Company, 1969.

VITA

John Robert Cass was born on 23 December, 1949 in San Benito, Texas. He graduated from Winston Churchill High School, San Antonio, Texas in 1967. He attended the Air Force Academy and graduated with a degree in Astronautical Engineering. He received a commission into the United States Air Force in June 1975. Pilot training was completed at Webb AFB, Texas where he received his wings in 1976. He became a T-38 instructor pilot at Vance AFB, Oklahoma until March 1980. He then served as a C-5 pilot in the 75th Military Airlift Squadron at Travis AFB, California before entering the School of Engineering at the Air Force Institute of Technology, Wright Patterson AFB, Ohio in June 1982.

Permanent Address: 4514 West 214th
Fairview Park, Ohio 44126

UNCLASSIFIED

SECURITY CLASSIFICATION OF THIS PAGE

REPORT DOCUMENTATION PAGE

1a. REPORT SECURITY CLASSIFICATION Unclassified	1b. RESTRICTIVE MARKINGS
2a. SECURITY CLASSIFICATION AUTHORITY	3. DISTRIBUTION/AVAILABILITY OF REPORT UNCLASSIFIED - DISTRIBUTION UNLIMITED
2b. DECLASSIFICATION/DOWNGRADING SCHEDULE	
4. PERFORMING ORGANIZATION REPORT NUMBER(S) AFIT/GA/AA/83D-1	5. MONITORING ORGANIZATION REPORT NUMBER(S)
6a. NAME OF PERFORMING ORGANIZATION School of Engineering 6b. OFFICE SYMBOL (If applicable) AFIT/EN	7a. NAME OF MONITORING ORGANIZATION
6c. ADDRESS (City, State and ZIP Code) Air Force Institute of Technology Wright-Patterson AFB, OH 45433	7b. ADDRESS (City, State and ZIP Code)
8a. NAME OF FUNDING/SPONSORING ORGANIZATION 8b. OFFICE SYMBOL (If applicable)	9. PROCUREMENT INSTRUMENT IDENTIFICATION NUMBER
8c. ADDRESS (City, State and ZIP Code)	10. SOURCE OF FUNDING NOS. PROGRAM ELEMENT NO. / PROJECT NO. / TASK NO. / WORK UNIT NO.
11. TITLE (Include Security Classification) DISCONTINUOUS LOW THRUST ORBIT TRANSFER (UNCLASSIFIED)	
12. PERSONAL AUTHOR(S) John R. Cass, Jr., B.S., Captain, USAF	
13a. TYPE OF REPORT MS Thesis 13b. TIME COVERED FROM _____ TO _____	14. DATE OF REPORT (Yr., Mo., Day) 1983 December 15. PAGE COUNT 64
16. SUPPLEMENTARY NOTATION	Approved for public release: IAW AFR 190-17. LYNN E. WOLAVER Dean for Research and Professional Development Air Force Institute of Technology (ATC) Wright-Patterson AFB OH 45433 3 JAN 1984

17. COSATI CODES		
FIELD	GROUP	SUB. GR.
22	03	

18. SUBJECT TERMS (Continue on reverse if necessary and identify by block number)
Low thrust
Electric propulsion
Orbital transfer

19. ABSTRACT (Continue on reverse if necessary and identify by block number)

Thesis Advisor: William E. Wiesel, Ph.D.

20. DISTRIBUTION/AVAILABILITY OF ABSTRACT UNCLASSIFIED/UNLIMITED ☒ SAME AS RPT. ☐ DTIC USERS ☐	21. ABSTRACT SECURITY CLASSIFICATION UNCLASSIFIED
22a. NAME OF RESPONSIBLE INDIVIDUAL William E. Wiesel, Ph.D., Associate Professor	22b. TELEPHONE NUMBER (Include Area Code) (513) 255-2109 22c. OFFICE SYMBOL AFIT/ENY

DD FORM 1473, 83 APR EDITION OF 1 JAN 73 IS OBSOLETE.

UNCLASSIFIED

SECURITY CLASSIFICATION OF THIS PAGE

This paper examines the use of discontinuous low thrust for orbital transfers between two non-coplanar, circular orbits. The vehicle is assumed to be a solar-powered, ion rocket that cannot operate when it is within the earth's shadow. Two timescales are used to derive a minimum fuel trajectory. The fast timescale solution maximizes a change in inclination when given a change in semi-major axis for a single orbit. The slow timescale solution combines fast timescale results to obtain the minimum fuel trajectory. Results are presented for three specific transfers requiring varying amounts of shadow penetration. It is shown that the fuel penalty caused by discontinuous thrust is small. However, there can be a moderate increase in total trip time if the time within the shadow is large.